Int J Earth Sci (Geol Rundsch) (2017) 106:939–958
DOI 10.1007/s00531-016-1342-z

ORIGINAL PAPER

Nature and evolution of lithospheric mantle beneath the southern Ethiopian rift zone: evidence from petrology and geochemistry of mantle xenoliths

Melesse Alemayehu[1,2] · Hong-Fu Zhang[1,3] · Patrick Asamoah Sakyi[4]

Received: 1 February 2016 / Accepted: 22 May 2016 / Published online: 1 June 2016

Abstract Mantle xenoliths hosted in Quaternary basaltic lavas from the Dillo and Megado areas of the southern Ethiopian rift are investigated to understand the geochemical composition and associated processes occurring in the lithospheric mantle beneath the region. The xenoliths are comprised of predominantly spinel lherzolite with subordinate harzburgite and clinopyroxenite. Fo content of olivine and Cr# of spinel for peridotites from both localities positively correlate and suggest the occurrence of variable degrees of partial melting and melt extraction. The clinopyroxene from lherzolites is both LREE depleted ($La/Sm_{(N)}$ = 0.11–0.37 × Cl) and LREE enriched ($La/Sm_{(N)}$ = 1.88–15.72 × Cl) with flat HREEs ($Dy/Lu_{(N)}$ = 0.96–1.31 × Cl). All clinopyroxene from the harzburgites and clinopyroxenites exhibits LREE-enriched ($La/Sm_{(N)}$ = 2.92–27.63.1 × Cl and, 0.45 and 1.38 × Cl, respectively) patterns with slight fractionation of HREE. The $^{143}Nd/^{144}Nd$ and $^{176}Hf/^{177}Hf$ ratios of clinopyroxene from lherzolite range from 0.51291 to 0.51370 and 0.28289 to 0.28385, respectively. Most of the samples define ages of 900 and 500 Ma on Sm–Nd and Lu–Hf reference isochrons, within the age range of Pan-African crustal formation. The initial Nd and Hf isotopic ratios were calculated at 1, 1.5, 2 and 2.5 Ga plot away from the trends defined by MORB, DMM and E-DMM which were determined from southern Ethiopian peridotites, thus indicating that the Dillo and Megado xenoliths could have been produced by melt extraction from the asthenosphere during the Pan-African orogenic event. There is no significant difference in $^{87}Sr/^{86}Sr$ ratios between the depleted and enriched clinopyroxene. This suggests that the melts that caused the enrichment of the clinopyroxene are mainly derived from the depleted asthenospheric mantle from which the xenoliths are extracted. Largely, the mineralogical and isotopic compositions of the xenoliths show heterogeneity of the CLM that could have been produced from various degrees of melt extraction, followed by metasomatism.

Keywords Dillo–Megado · Mantle xenoliths · Depletion · Enrichment · Sr–Nd–Hf isotopes

Electronic supplementary material The online version of this article (doi:10.1007/s00531-016-1342-z) contains supplementary material, which is available to authorized users.

✉ Melesse Alemayehu
melesse555@yahoo.com

✉ Hong-Fu Zhang
hfzhang@mail.igcas.ac.cn

[1] State Key Laboratory of Lithospheric Evolution, Institute of Geology and Geophysics, Chinese Academy of Sciences, P.O. Box 9825, Beijing 100029, China

[2] Department of Earth Science, School of Earth Science and Mining Engineering, Addis Ababa Science and Technology University, P.O. Box 16417, Addis Ababa, Ethiopia

[3] State Key Laboratory of Continental Dynamics, Department of Geology, Northwest University, Xi'an 710069, China

[4] Department of Earth Science, University of Ghana, P.O. Box LG 58, Legon-Accra, Ghana

Introduction

The East Africa Rift System (EARS) is the largest region in Africa where the contribution of active magmatism on continental lithospheric mantle (CLM) can be constrained using information from mantle xenoliths. The CLM of the EARS has experienced multiple tectonic processes, for example, Pan-African subduction and Cenozoic East

African rifting. Studies of mantle-derived rocks (e.g., basalts) available at the surface are complementary to understanding mantle sources and processes happening at depth, for which no direct samples are available. The evidence of lithospheric mantle processes beneath the EARS has usually been investigated via elemental and radiogenic isotope compositions of volcanic rocks (e.g., Kieffer et al. 2004; Rooney et al. 2005; Tommasini et al. 2005; Furman et al. 2006; Ferrando et al. 2008; Ayalew et al. 2009; Beccaluva et al. 2009; Frezzotti et al. 2010). However, much of the knowledge about the nature and evolution of the CLM comes from direct samples like mantle xenoliths carried to the surface by volcanic rocks of the EARS (Courtillot et al. 2003).

Mantle xenoliths from continental areas usually document a complex element depletion and enrichment history of CLM (Sun and McDonough 1989; Pearson 1999). Depleted mantle signatures of minerals from mantle xenoliths are mostly rare, and mantle xenoliths almost always require some degree of enrichment (metasomatism) to explain their characteristics (e.g., Nasir et al. 2006; Zhang et al. 2010; Tang et al. 2008). Various types of metasomatic fluids/melts ranging from H_2O- and CO_2-rich fluids to silicate- and carbonate-rich melts have been described using trace element distributions in clinopyroxene (e.g., Coltorti et al. 1999). Clinopyroxene characterized by higher Ti/Eu and lower $(La/Yb)_N$ implies that the metasomatic agent was a silica-rich melt (or fluid) rather than a carbonate-rich fluid (Yaxley et al. 1991; Rudnick et al. 1993; Coltorti et al. 1999).

The Ethiopian Cenozoic lavas contain various types of mantle xenoliths ranging from spinel bearing lherzolite, harzburgite, websterite to garnet pyroxenite (Rogers et al. 1999; Conticelli et al. 1999; Ayalew et al. 2003; Reisberg et al. 2004; Ferrando et al. 2008; Ayalew et al. 2009; Frezzotti et al. 2010; Alemayehu et al. 2010; Alemayehu 2010; Meshesha et al. 2011; Beccaluva et al. 2011; Bianchini et al. 2014; Alemayehu et al. 2016a, b, c). Previous geochemical studies of Ethiopian mantle xenoliths reported a suite of compositionally different mantle xenoliths that characterize variably depleted and enriched portions of the CLM of Ethiopia (Meshesha et al. 2011; Bianchini et al. 2014; Alemayehu et al. 2015, 2016a). Previous studies also proposed that the formation of the Ethiopian CLM protolith from an already depleted mantle source occurred during the accretion and growth of the Pan-African crust at about 900–500 Ma, which is similar to the Arabian lithospheric mantle (McGuire 1988; Nasir 1992; Abdelsalam and Stern 1996). However, Re–Os and Lu–Hf isotopes from the peridotites showed that melt extraction from the CLM of the southern Ethiopia rift took place between 0.9 and 2.8 Ga (Reisberg et al. 2004; Meshesha et al. 2011; Bianchini et al. 2014).

On a global scale, compositional changes in the lithospheric mantle are caused by peridotite–melt interaction. The melts that modify its composition may come from crustal materials and/or the asthenosphere. The interaction of peridotites with melts from different sources results in compositional changes and the formation of new minerals (Zhang et al. 2008). Thus, geochemical studies of peridotite–melt interaction processes can shed light on the evolution and compositional heterogeneity of the lithospheric mantle in extensional settings (Piccardo et al. 2004; Rampone et al. 2004) like that of the EARS. Recent studies have revealed that most peridotites are affected by various stages of peridotite–melt interaction, occurring at different lithospheric levels and causing significant geochemical modifications of the lithospheric mantle (Piccardo et al. 2007). Peridotite–melt interactions that occur in the Ethiopia CLM have been identified to be the result of multiple metasomatic overprints, initially associated with Pan-African accretion and subsequently by small degree melts from asthenospheric or plume mantle sources during East African rift development (Rogers et al. 1999; Beccaluva et al. 2011). In order to understand the composition and influence of peridotite–melt interaction in the CLM of the southern Ethiopian rift, we combine petrography with elemental and isotope geochemistry to understand the extent of peridotite–melt reactions and related processes preserved in Dillo and Megado mantle xenoliths. Moreover, this is the first Sr, Nd and Hf isotopic study for the Megado xenoliths, as well as the first Hf isotopic study for the Dillo xenoliths.

Geological setting and sample description

Geological setting

The Main Ethiopian Rift (MER) intersects with two oceanic rifts (Red Sea and Gulf of Aden) at the Afar depression and is oriented NNE–SSW (Merla et al. 1973; Fig. 1). It has three segments, namely northern, central and southern, and begins at the Afar depression trending toward the south. The southern MER is about 300 km wide, composed of half and full grabens and considered basin and range style tectonics (Yemane et al. 1999). Volcanic rocks overlie Late Proterozoic basement and are associated with a thin layer of Early Tertiary sandstone (Davidson 1983). The volcanic rocks have Late Eocene to Plio-Pleistocene ages and are up to 1 km thick (Ebinger et al. 1993). These volcanic rocks are composed of transitional tholeiitic basalts and pyroclastics and are mainly exposed in Amaro, Gamo, Gidole and around the Chew Bahir areas (Ebinger et al. 1993). Miocene volcanism (19–11 Ma) formed a large volume of alkali basalts and trachytes that are similar to the syn-rift volcanics of the MER (Ebinger et al. 1993).

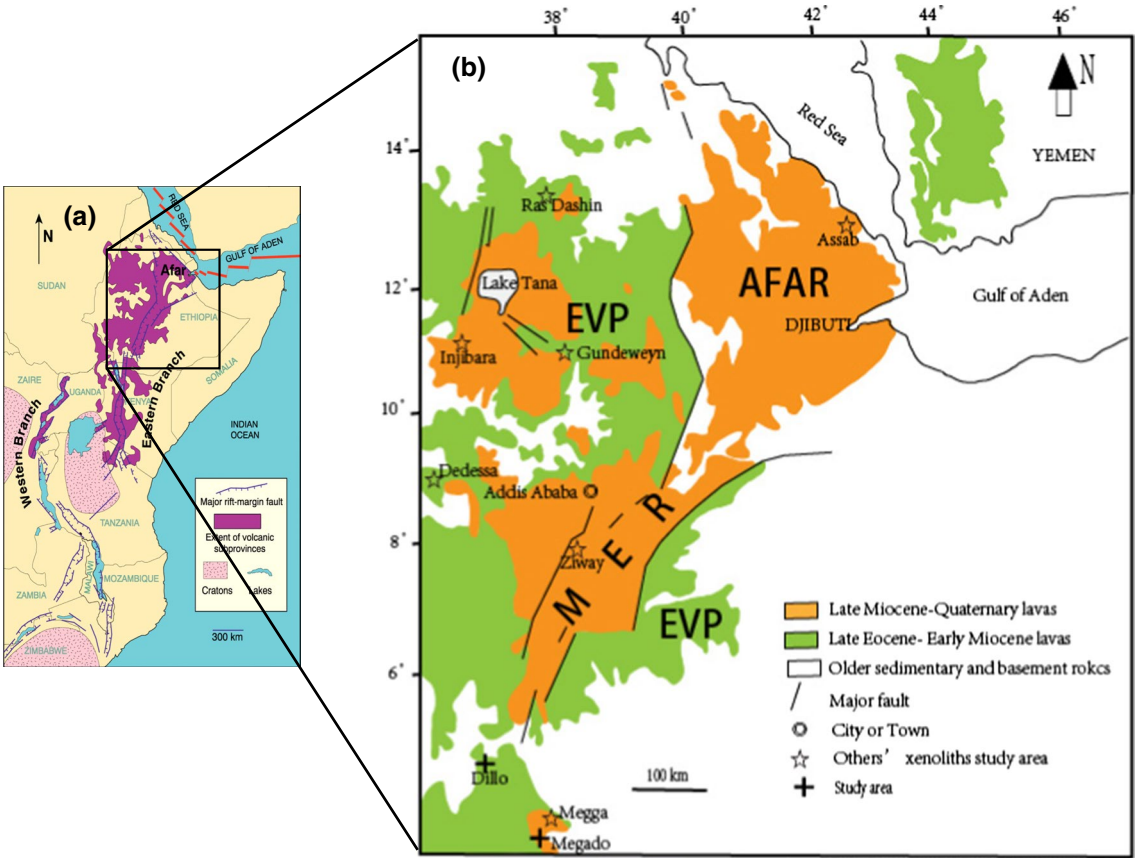

Fig. 1 **a** The distribution of Neoproterozoic basement rocks (Kampunzu and Mohr 1991), **b** the location of study area and distribution of mantle xenoliths in Ethiopia (Ferrando et al. 2008). The MER and EVP denote the Main Ethiopian Rift and Ethiopian volcanic province, respectively. The locations of the study areas are shown by a cross (+)

Plio-Pleistocene volcanism was mostly limited to the axial zones of the rift (Yemane et al. 1999). Nevertheless, magmatism produced away from the axial zones in the adjacent highlands in southern MER has been reported by Davidson and Rex (1980). These rocks are basaltic in composition and occur as lava flows, spatter cones, scoria cones and maars. They are mostly associated with pyroclastic deposits and minor phonolites, trachytes and rhyolites. Generally, three types of volcanic rocks are described from southern MER based on K–Ar ages. These are (1) Miocene (10.5–12.7 Ma) alkali basalts, (2) Pliocene (3.6–4.7 Ma) tholeiitic basalts and (3) Quaternary (0.2–1.9 Ma) alkaline basalts (Davidson 1983). Among the three, the Quaternary basalts enclose several types of fresh mantle xenoliths (Rogers et al. 1999; Orlando et al. 2006; Meshesha et al. 2011).

Sample description

Our samples were collected from Cenozoic basaltic lava flows (1.9–0.3 Ma; Shinjo et al. 2010) that lie in the southern margin of the MER from the Dillo and Megado areas, which are about 70 km apart and 550 km south of Addis Ababa (Fig. 1b; Supplementary Table 1). The basalts contain both tholeiitic and alkaline types. The alkaline basalts carry abundant mantle xenoliths that have protogranular and porphyroclastic textures. Most of the samples are lherzolites; however, some harzburgites and olivine clinopyroxenites are present from Megado. The geochemical compositions of Dillo and Megado xenoliths are markedly different from cratonic mantle lithosphere found beneath other Archean cratons (e.g., Rudnick et al. 2004) and fall with the compositional range of off-cratonic and other Ethiopian mantle xenoliths (Fig. 3) (Rogers et al. 1999; Conticelli et al. 1999; Meshesha et al. 2011; Beccaluva et al. 2011; Bianchini et al. 2014; Alemayehu et al. 2016b). Sm–Nd, Lu–Hf and Re–Os isotopes of southern Ethiopia peridotites generated a poorly constrained age range of 0.9–2.8 Ga (Reisberg et al. 2004; Meshesha et al. 2011; Bianchini et al. 2014). Trace element and Sr–Nd–Pb isotopic compositions of the peridotites reflect various types of metasomatic overprinting (Meshesha et al. 2011). A more complete discussion on the petrography and compositional descriptions of the samples is provided in "Results" section.

Analytical methods

Sample analyses were conducted at the State Key Laboratory of Lithospheric Evolution, Institute of Geology and Geophysics, Chinese Academy of Sciences, Beijing, China. A conventional optical microscope was used to describe thin section petrography. The electron microprobe analyses were performed using a JEOL JXA-8100 on polished and carbon-coated thin sections to determine major element compositions of different minerals. The analytical procedures were carried with counting times of 10–30 s for each peak with an accelerating voltage of 15 kV, a beam current of 10 nA and a beam size of 5 μm. For standard calibration, natural and synthetic minerals were used. Jadeite for Na, Al and Si; rhodonite for Mn; sanidine for K; garnet for Fe; Cr-diopside for Ca; and olivine for Mg were used as natural standards, while rutile for Ti, 99.7 % chromium(III) oxide for Cr and Ni_2Si for Ni were used as synthetic standards. The ZAF procedure was used to correct the raw data, and the precision for all analyzed elements was better than 98 %. From each sample, three grains were analyzed for each mineral. Laser ablation inductively coupled plasma mass spectrometry used an Agilent 7500cs to determine trace element abundances in clinopyroxene. To enhance the transport efficiency of the ablated sample, helium was used as a carrier gas. The helium carrier gas inside the ablation cell was mixed with argon before entering the ICP in order to maintain a stable and optimum excitation condition. The measurements were taken using time-resolved analysis, operating in a fast peak-hopping sequence in dual detector mode. The analytical spot size was 40 μm, and each spot analysis consisted of c. 30 s of background acquisition followed by 60 s of data acquisition. The NIST 610 glass was used as an external standard. The CaO determined by the electron microprobe was used as the internal standard. Data reduction was carried out using the software GLITTER, version 4. The measured values of NIST 610 were in satisfactory agreement with the recommended values (Pearce et al. 1997). Precision and accuracy, better than 10 % for most elements, were assessed by repeated analyses of NIST 612. Detection limits were typically in the range 10–100 ppb for Rb, Sr, Zr, Cs, Ba, Gd and Pb, 1–10 ppb for Y, Nb, La, Ce, Nd, Sm, Eu, Tb, Dy, Er, Yb, Hf and Ta and usually <1 ppb for Pr, Ho, Tm, Lu, Th and U. More information on instrument operating conditions and calibration values for the LA-ICP system is reported in Liu et al. (2008) and Chen et al. (2011).

For Sr–Nd–Hf isotope analysis, clinopyroxene separates were acid-leached in 6 M HCl for 8 h at 80 °C (Tanaka and Nakamura 2002) prior to acid digestion. The leaching was done to remove any contaminants associated with grain boundaries and grain surface. After leaching, the residue was dried and weighed (ca. 100–200 mg) in a Teflon beaker, and the samples were dissolved in a mixture of concentrated $HF–HNO_3–HClO_4$ (Yang et al. 2010) with Rb, Sr, Lu, Hf spikes and Sm–Nd mix spikes. All isotope analyses, including chemical separation and mass spectrometry, were performed following the methods of Yang et al. (2010). The abundance of Rb, Sr, Sm and Nd, and Sr–Nd isotope composition was determined by thermal ionization mass spectrometry (Finnigan MAT 262). The instrumental mass fractionation was corrected by normalizing $^{86}Sr/^{88}Sr$ and $^{146}Nd/^{144}Nd$ to 0.1194 and 0.7219, respectively (O'Nions et al. 1979; Wasserburg et al. 1981). During the period of data collection, the measured values for the NBS-987 Sr standard and the JNdi-1 Nd standard were $^{87}Sr/^{86}Sr = 0.710265 \pm 16$ (2 s, $n = 4$) and $^{143}Nd/^{144}Nd = 0.512125 \pm 12$ (2 s, $n = 4$), respectively, which fall within uncertainty of the recommended values ($^{87}Sr/^{86}Sr = 0.710256 \pm 16$, Li et al. 2012; $^{143}Nd/^{144}Nd = 0.512123 \pm 15$; Li et al. 2007). The abundances of Lu and Hf, and Hf isotope composition were determined with multi-collector ICP-MS (MC-ICPMS, Thermo Neptune) following procedures described in Yang et al. (2010). The $^{176}Hf/^{177}Hf$ ratios were normalized to 0.7325 to correct instrumental mass fractionation, and $^{176}Lu/^{175}Lu$ isotopic ratios were normalized using Yb isotopic ratios. The standard Alfa Hf was measured during the analysis, and the average value of $^{176}Hf/^{177}Hf$ was 0.282195 ± 13 (2 s, $n = 10$), which falls within uncertainty of the recommended values ($^{176}Hf/^{177}Hf = 0.282189 \pm 19$, Yang et al. 2010). The USGS reference material BCR-2 was measured for Sr, Nd and Hf isotopic composition to monitor the accuracy of the analytical procedures, with the following results: $^{87}Sr/^{86}Sr = 0.704986 \pm 13$ (2 s), $^{143}Nd/^{144}Nd = 0.512623 \pm 13$ (2 s) and $^{176}Hf/^{177}Hf = 0.282880 \pm 14$ (2 s). These values are comparable to the reported BCR-2 reference values ($^{87}Sr/^{86}Sr = 0.705003 \pm 20$, Raczek et al. 2003; $^{143}Nd/^{144}Nd = 0.512632 \pm 20$, Li et al. 2007; $^{176}Hf/^{177}Hf = 0.282884 \pm 20$, Le Fevre and Pin 2001). Depleted parameters applied in the determination of Nd and Hf model ages were $^{147}Sm/^{144}Nd = 0.222$, $^{143}Nd/^{144}Nd = 0.513114$, $^{176}Lu/^{177}Hf = 0.03915$ and $^{176}Hf/^{177}Hf = 0.2833$ (Vervoort et al. 1999). In the calculation, the following decay constants were used: $^{147}Sm = 6.54 \times 10^{-12}$/year and $^{176}Lu = 1.94 \times 10^{-11}$/year. The bulk earth parameters applied in the calculation of εNd are $^{147}Sm/^{144}Nd = 0.1967$ and $^{143}Nd/^{144}Nd = 0.512638$ (Goldstein et al. 1984), and those of εHf are $^{176}Lu/^{177}Hf = 0.0332$ and $^{176}Hf/^{177}Hf = 0.282772$ (Vervoort et al. 1999).

Results

Petrography

The xenoliths hosted in basaltic lavas are very fresh, vary from 5 to 30 cm in the longest dimension (Fig. 2a–c) and are composed of four mineral phases, namely olivine, orthopyroxene, clinopyroxene and spinel. Sulfide minerals occur in some Megado xenoliths, but no hydrous minerals were observed even though Orlando et al. (2006) and Meshesha et al. (2011) have previously reported the presence of amphibole in the Dillo and Megado mantle xenoliths. Most of the Megado xenoliths are categorized as lherzolite with minor harzburgite and olivine clinopyroxenite (Fig. 2d). The peridotites show protogranular to porphyroclastic primary textures (Mercier and Nicolas 1975; Fig. 3a, b). Secondary textures including lamellae, reactions, spongy and fluid inclusions are also present in a few xenoliths (Fig. 3c–h). The lamellae textures are more prominent in xenoliths from Dillo than those from Megado, which are dominated by reaction textures. All of the Dillo xenoliths are lherzolites.

Spinel lherzolites from both localities occur with protogranular and porphyroclastic textures. The minerals are anhedral to subhedral (2–5 mm). Some olivine grains exhibit kink banding oriented parallel to the grain elongation. Furthermore, coarse-grained olivine illustrates undulatory extinction. In some cases, rounded olivine up to 1 mm in size occurs as inclusions in orthopyroxene. Orthopyroxene in the protogranular and porphyroclastic lherzolite is anhedral to subhedral, varying in size from 1 to 3 mm. Some orthopyroxene contains thin elongated lamellae of clinopyroxene. The clinopyroxene from protogranular and porphyroclastic lherzolite is 1–3 mm in size with exsolution lamellae of orthopyroxene and occasional fluid inclusions; this feature is mostly found in the

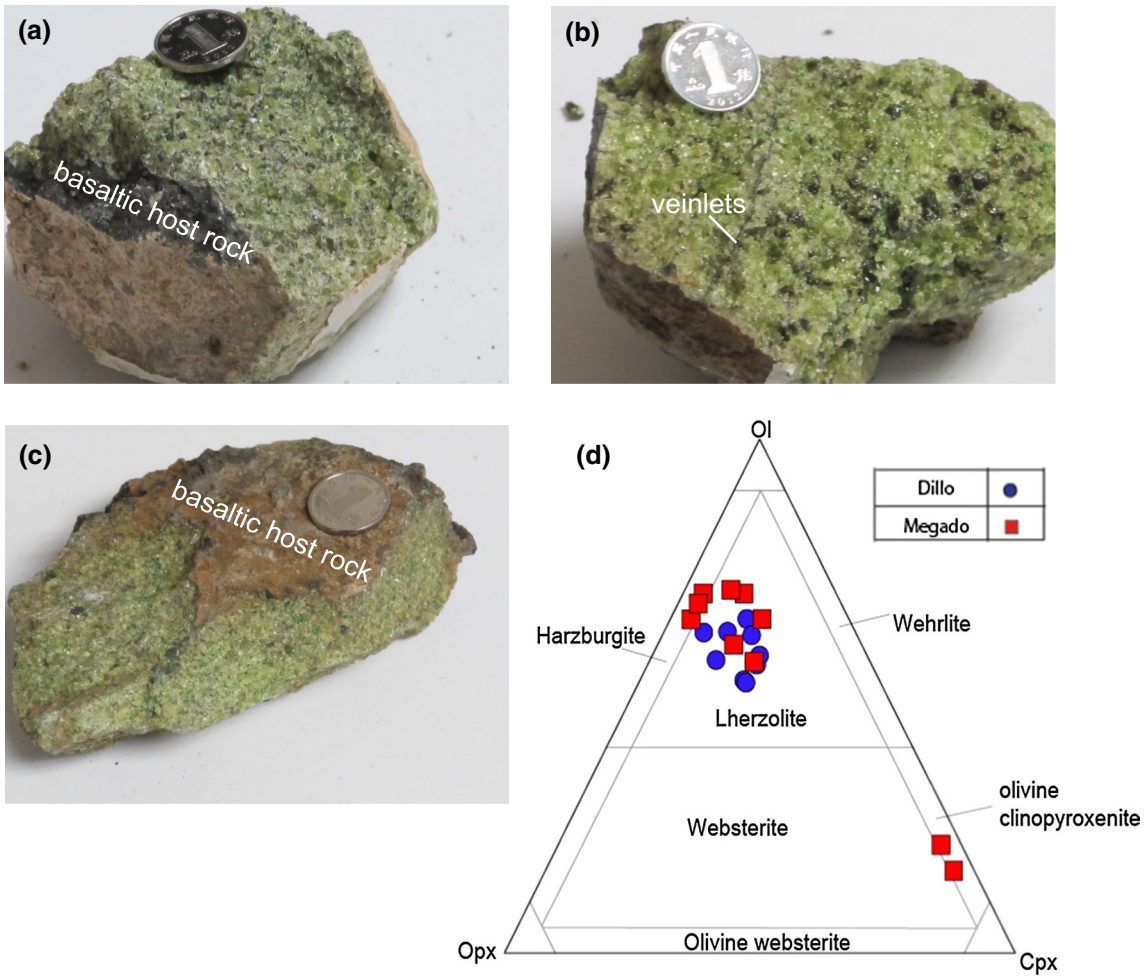

Fig. 2 Hand specimens of mantle xenoliths showing *greenish* fresh color **a** spinel lherzolite from Dillo, DL56, **b** spinel harzburgite from Megado, MG55, **c** spinel olivine clinopyroxenite from Megado, MG80. **d** Classification of the xenoliths (after Streckeisen 1976). Ol, Opx and Cpx denote olivine, orthopyroxene and clinopyroxene, respectively

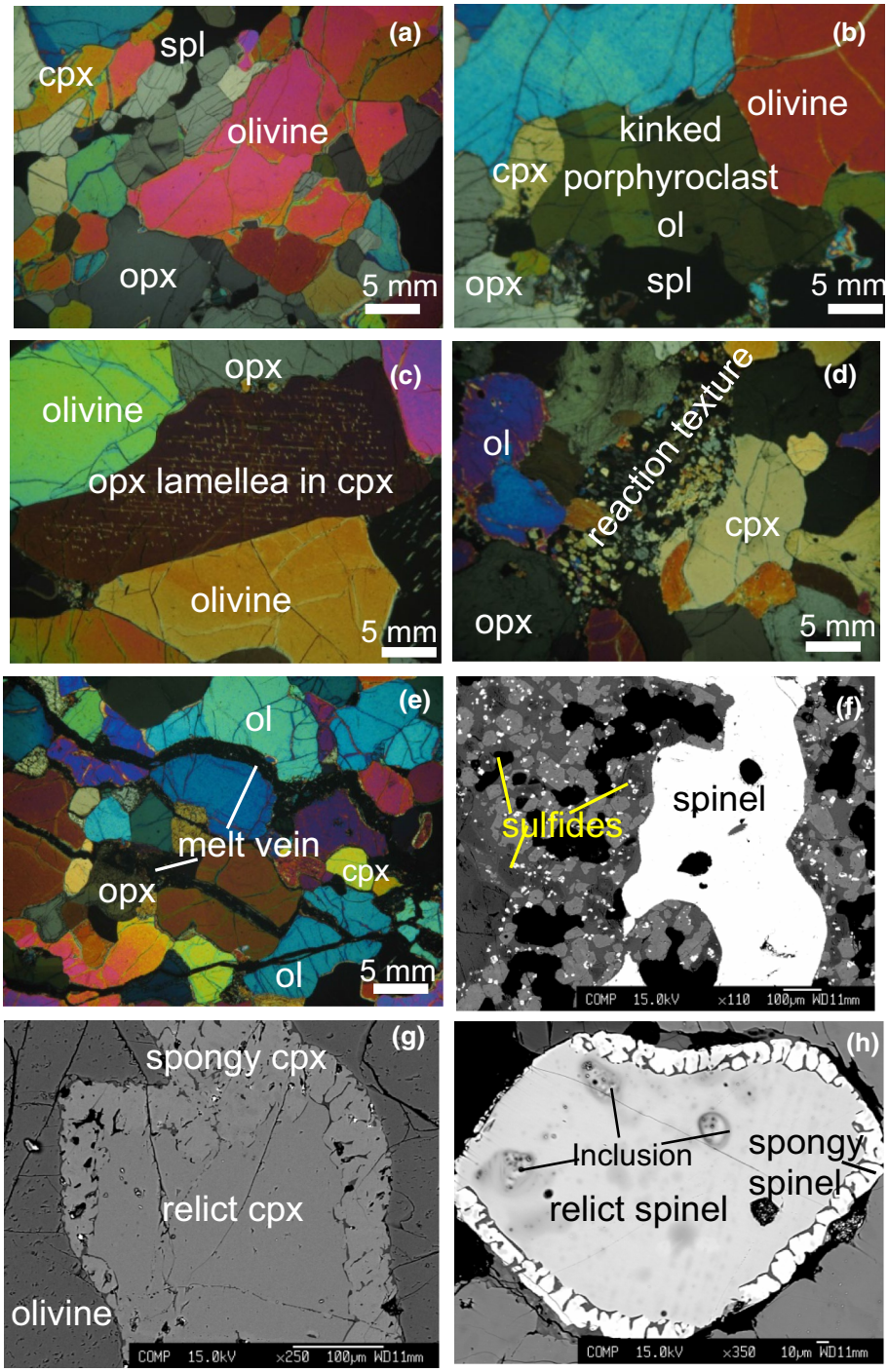

Fig. 3 **a** Protogranular texture with coarse- and fine-grained layering, **b** porphyroclastic texture and kinked olivine with zigzag grain boundaries, **c** lamellae of orthopyroxene exsolved from clinopyroxene, **d** the mineral assemblages and reaction textures in olivine clinopyroxenite from sample MG82, **e** basaltic melt veins containing orthopyroxene, clinopyroxene and plagioclase, and with reaction textures at the minerals contacts, **f** dense distribution of very small white sulfide minerals in harzburgite, **g** spongy clinopyroxene composed of relict clinopyroxene in the center with a spongy rim that contains secondary clinopyroxene and glass, **h** spongy spinel composed of relict spinel and fluid inclusions in the center. **a**–**e** = cross-polarized light images and **f**–**h** = back-scattered electron (BSE) images. Olivine, orthopyroxene, clinopyroxene and spinel are denoted by ol, opx, cpx and spl, respectively

Dillo xenoliths. Spinel is reddish brown, is anhedral, ranges from 0.1 to 1 mm and shows a thin alteration on its grain boundaries. In rare cases, strained and aligned spinel forms a foliation. Spinel harzburgites from Megado show coarse-grained protogranular to porphyroclastic textures, while olivine occurs as anhedral to subhedral grains up to 5 mm in size and exhibits kink bands. The clinopyroxene exsolution lamellae are found in large orthopyroxene that measure up to 4 mm in size, whereas the clinopyroxene is usually small (up to 2 mm). Vermicular and reddish brown spinel is surrounded by fine aggregates of olivine and pyroxene (0.1–1 mm). The Megado harzburgites contain enormous euhedral to anhedral sulfide grains enclosed in olivine and pyroxene, as well as at the grain boundaries (Fig. 3f). Two olivine clinopyroxenites from Megado show coarse-grained protogranular to porphyroclastic textures. Olivine occurs as anhedral to subhedral grains up to 5 mm and exhibits kink bands. Orthopyroxene is rare and small (up

to 1 mm). Clinopyroxene is anhedral to subhedral and often contains lamellae of orthopyroxene. Reddish brown spinel is surrounded by fine aggregates of olivine and pyroxene (0.1–1 mm). Consequently, clinopyroxenite was used instead of olivine clinopyroxenite for convenience.

Reaction textures containing melt pockets and veinlets mostly occur in the Megado xenoliths. These textures are often found between pyroxene and olivine, and they occur as rims or crosscutting veinlets and patches commonly associated with pools of amorphous glassy material. The reaction texture consists of an aggregate of olivine, orthopyroxene, clinopyroxene and a trace amount of Fe–Ti oxide (Fig. 3d, e). The spongy texture usually occurs as rims or coronae on clinopyroxene and spinel in most of the mantle xenoliths (Fig. 3g, h). Secondary clinopyroxene and amorphous basaltic glass pockets typically fill the spongy regions. A few melt and/or fluid inclusions are present in silicate phases, dominantly in clinopyroxenite. The inclusions are randomly distributed within olivine, orthopyroxene, clinopyroxene and spinel (Fig. 3h).

Major element compositions

To examine the compositional variations in olivine, orthopyroxene, clinopyroxene and spinel, backscattered electron elemental maps were obtained. The minerals are homogeneous from core to rim in major oxides, and the average major element composition is given in Supplementary Table 1.

Olivine and spinel

Olivine forsterite (Fo) equivalent to Mg# [Mg# = 100 × Mg/(Mg + Fe)] is 88.4–89.5 for Dillo and 89.0–91.4 for Megado xenoliths. The concentration of NiO ranges from 0.32 to 0.40 wt% and falls within the range of Type I xenoliths (0.30–0.54 wt%: Frey and Prinz 1978). All lherzolites and some harzburgites fall within the field of Phanerozoic and Proterozoic lherzolites, respectively (Griffin et al. 1998). The olivine from the lherzolites and harzburgites defines a trend of increasing Fo content with increasing modal olivine (Fig. 4a), which is similar to the oceanic trend (Boyd 1998). Spinel is characterized by a range in Cr# [Cr# = 100 × Cr/(Cr + Al)] of 8.1–59.3. The lowest and highest Cr# of spinel was, respectively, observed in the Dillo lherzolite and Megado harzburgite. The Cr# of spinel decreases with increasing modal abundance of clinopyroxene and correlates with the Fo content within the olivine–spinel mantle array (OSMA; Arai 1994; Fig. 4b). All lherzolites in this study plot within the low Cr# field in the OSMA, but the harzburgites and clinopyroxenites plot toward high Cr# values (Fig. 4b).

Pyroxene

Orthopyroxene and clinopyroxene are characterized by high Mg# and are classified as enstatite and diopside (Morimoto 1988; Supplementary Table 1). The Mg# of orthopyroxene varies from 89.2 to 91.5 for Dillo and 89.0–91.4 for Megado xenoliths. The orthopyroxenes from the harzburgite and clinopyroxenite tend to have higher Mg# and Cr_2O_3 than those from the lherzolite, and they show the lowest Al_2O_3 and TiO_2 abundances which overlap with the composition of off-cratonic peridotites (Fig. 4c). Most of the clinopyroxene with high Mg# is found in the harzburgite (91.2–92.8) and clinopyroxenite (91.9–92.6), whereas the clinopyroxene with the lowest Mg# of 89.0 occurs in the Dillo lherzolite. The clinopyroxene from harzburgite and clinopyroxenite contains more Cr_2O_3 than those in the lherzolite. The Al_2O_3 contents of clinopyroxene range from 5.47 to 7.21 wt% for Dillo and 2.03 to 6.62 wt% for Megado xenoliths. It should be noted that the clinopyroxene with the highest and lowest Al_2O_3 contents occurs in the Dillo lherzolite and Megado clinopyroxenite, respectively. Similarly, clinopyroxene with the highest (2 wt%) and lowest (0.96 wt%) Na_2O content is found in the Dillo lherzolite and Megado harzburgite, respectively. Additionally, clinopyroxene from the Dillo peridotites contains higher TiO_2 than that from their Megado counterparts. The compositions of most clinopyroxene from the lherzolite fall within the fertile region, whereas the clinopyroxene from the harzburgite and clinopyroxenite trends into the refractory field (Fig. 4d; Zheng et al. 2001).

Geothermobarometry

Equilibrium temperatures were calculated using Wells (1977), Sachtleben and Seck (1981), Brey and Kohler (1990), Witt-Eickschen and Seck (1991), Nimis and Taylor (2000) and MacGregor (2015–2016). These thermometers typically give a temperature discrepancy of 20–100 °C (Supplementary Table 2). Recent studies proposed that the orthopyroxene geothermometer and associated orthopyroxene solvus geobarometer give the best estimates of mantle temperature–pressure conditions (MacGregor 2015), and these were employed in this study. It is notable that the temperature and pressure estimated for mantle xenoliths from both localities do not show any systematic difference. The estimated equilibrium temperature and pressure for the Dillo and Megado xenoliths are 852–965 °C and 13.1–14.4 kbar and 800–905 °C and 9.9–13.3 kbar, respectively (Supplementary Table 2). The lowest temperature and pressure were obtained from the Megado clinopyroxenite. All the Ethiopian plateau and rift xenoliths, including those from this study, lie between the 60 and 150 mW/m^2

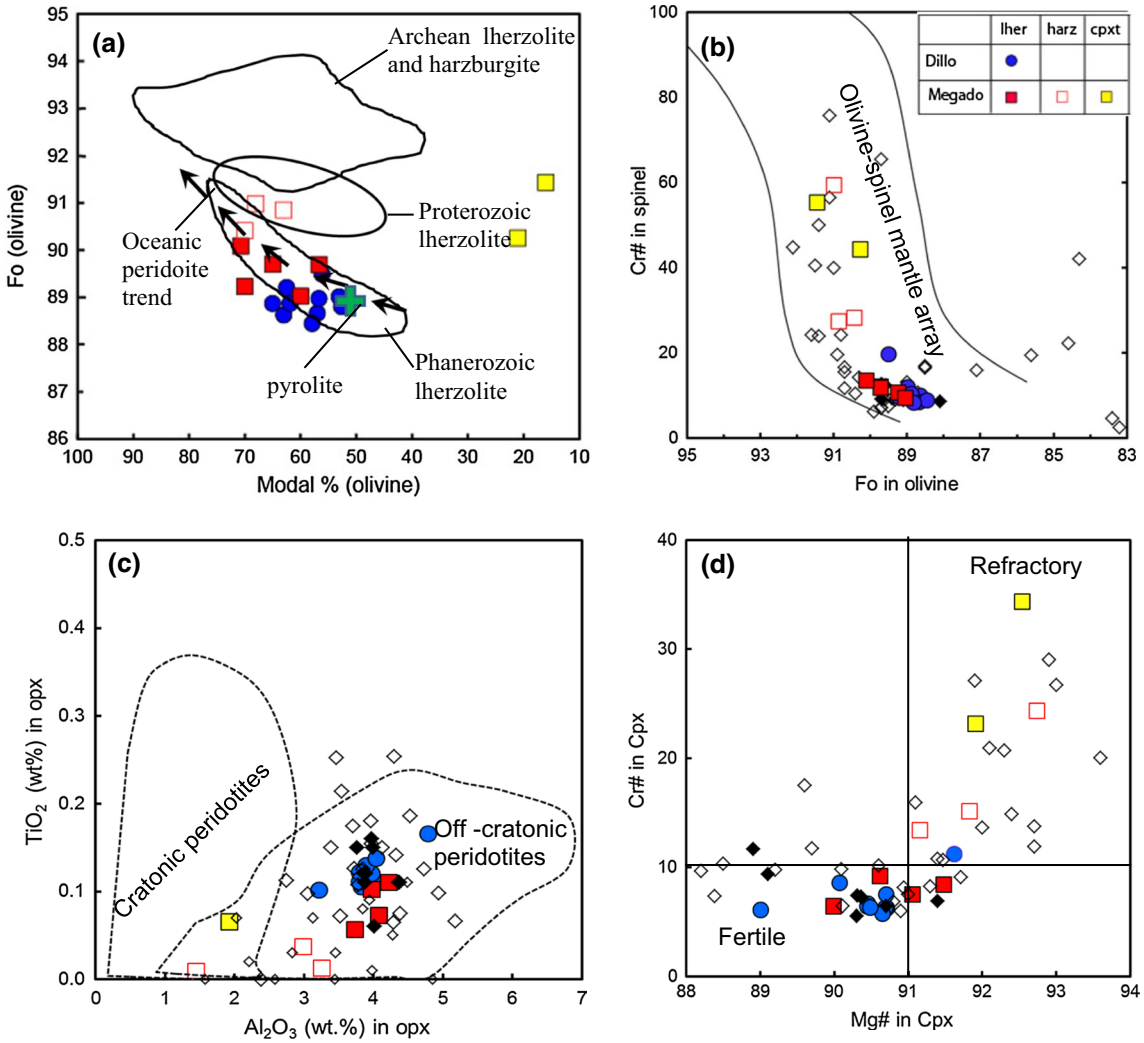

Fig. 4 Olivine, orthopyroxene, and clinopyroxene and spinel compositions in lherzolite, harzburgite and clinopyroxenite from the Dillo and Megado mantle xenoliths compared with Ethiopian rift and plateau xenoliths. (**a**) Modal olivine content versus Fo content of olivine. The depletion trend for oceanic-peridotite is from Boyd (1998). The fields of Archean, Proterozoic and Phanerozoic are from Griffin et al. (1998). (**b**) Fo content of olivine versus Cr# of coexisting spinel, (**c**) Al_2O_3 versus TiO_2 (wt%) in opx and (**d**) Mg# versus Cr# in cpx. Olivine–spinel mantle array (OSMA) is from Arai (1994), cratonic and off-cratonic fields are from Rudnick et al. (2004), and the fields for fertile and refractory mantle regions are from Zheng et al. (2001). Filled and unfilled diamond symbols are data of Ethiopian plateau and rift xenoliths, respectively (Bedini et al. 1997; Rogers et al. 1999; Bedini and Bodinier 1999; Conticelli et al. 1999; Lorand et al. 2003; Rooney et al. 2005; Ferrando et al. 2008; Ayalew et al. 2009; Beccaluva et al. 2009; Teklay et al. 2010; Frezzotti et al. 2010; Meshesha et al. 2011; Bianchini et al. 2014). The lherzolite, harzburgite and olivine clinopyroxenite are denoted in the legend table as lherz, harz and cpxt, respectively. The circle and square symbols represent the Dillo and Megado localities, respectively. All abbreviations are the same as in Fig. 2

geothermal gradients (Fig. 5), which are not common for continental environments (40 mW/m^2; Pollack and Chapman 1977). Moreover, there is no clear correlation between temperature and pressure for the major element compositions among the different types of xenoliths.

Trace element compositions

The in situ trace element compositions of clinopyroxene are given in Supplementary Table 3, and their chondrite and primitive mantle-normalized plots are summarized in Fig. 6. There is no significant difference between inter- and intragrain trace element compositions. Two groups of clinopyroxene from both Dillo and Megado xenoliths are observed based on LREE/M-HREE ratios (terminology of Frey and Martin 1978). These are LREE-enriched (enriched) and LREE-depleted (depleted) types. The trace element compositions of the Dillo and Megado clinopyroxene fall within the field defined by Arabian xenoliths (Fig. 6; Shaw et al. 2007; Nasir and Rollinson 2009; Nasir and Stern 2012).

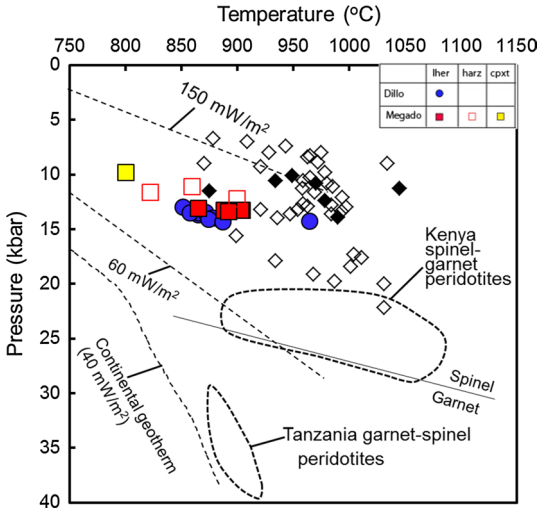

Fig. 5 Temperature (°C) and pressure (kbar) equilibrium conditions estimated for the Dillo and Megado xenoliths using the Cr solubility in orthopyroxene geothermometer and associated orthopyroxene solvus geobarometer (MacGregor 2015–2016). Geothermal gradients of 40, 60 and 150 W/m^2 heat flow are from Pollack and Chapman (1977). Data sources for plateau and rift xenoliths are from Bedini et al. (1997), Rogers et al. (1999), Conticelli et al. (1999), Rooney et al. (2005), Teklay et al. (2010), Ayalew et al. (2009) and Meshesha et al. (2011). Tanzanian xenoliths are from Lee and Rudnick (1999), and Kenyan xenoliths are from Kaeser et al. (2009). The *circle* and *square* symbols represent the Dillo and Megado localities, respectively

Lherzolite

On a chondrite-normalized diagram (Fig. 6a), clinopyroxene from Dillo and Megado lherzolite shows two distinct trends. One trend is depleted in LREE ($La/Sm_{(N)}$ = 0.11–0.37 × Cl) with flat HREE ($Dy/Lu_{(N)}$ = 0.96–1.31 × Cl), whereas the other shows enrichment in LREE ($La/Sm_{(N)}$ = 1.88–15.72 × Cl). One exception is a sample from Dillo that also has lower abundances of HREE ($Dy/Lu_{(N)}$ = 0.72 × Cl) relative to the other samples (Fig. 6a). On multi-trace element patterns normalized to primitive mantle (Fig. 6b), clinopyroxene from lherzolite has negative Ba and Nb anomalies relative to adjacent elements. Some enriched samples show high abundance of Th (up to 434.7 × PM) and U (up to 185.1 × PM). Abundances of Y, Zr and Hf are similar between depleted and enriched samples (Fig. 6b) with the exception of the enriched Dillo lherzolite, in which depleted and enriched clinopyroxene shows negative Li anomalies relative to the adjacent REE (Fig. 6b).

Harzburgite

Clinopyroxene from all harzburgites (Fig. 6c, d) exhibits different REE profiles compared to those in the lherzolites. Clinopyroxene samples are enriched in LREE ($La/Sm_{(N)}$ = 2.92–27.63.1 × Cl) with slight fractionation of HREE ($Dy/Lu_{(N)}$ = 0.98–1.31 × Cl). A strong negative anomaly in Sm relative to the adjacent REEs is present in one sample (MG55). On a primitive mantle-normalized multi-trace element diagram (Fig. 6d), the harzburgite is depleted in Nb, Ta, Zr and Hf relative to adjacent elements. A slight positive Th spike is also present (Fig. 6d).

Clinopyroxenite

The clinopyroxene from Megado clinopyroxenites displays distinct REE patterns than the lherzolites, but similar to the harzburgites (Fig. 6e, f). The two clinopyroxene samples are enriched in LREE ($La/Sm_{(N)}$ = 0.45 and 1.38 × Cl) with slight fractionation of HREE ($Dy/Lu_{(N)}$ = 2.47 and 4.21 × Cl). The multi-trace element pattern is depleted in Ba, Nb, Hf and Li relative to adjacent elements. The abundance of Th (1.28 and 20.43 × PM) and U (3.97 and 6.97 × PM) in clinopyroxene is lower compared with the harzburgite (Th up to 50 × PM and U up to 17.41 × PM) (Fig. 6f).

Sr, Nd and Hf isotope compositions

The results of Sr, Nd and Hf isotopic analyses of clinopyroxene are given in Supplementary Table 4 and plotted in Fig. 7. Clinopyroxene from the depleted and enriched lherzolite groups shows similar Sr and Nd isotopic ratios. The $^{87}Sr/^{86}Sr$ ratio varies from 0.70198 to 0.70293 for Dillo and 0.70224 to 0.70301 for Megado clinopyroxene. The Dillo defines a broader $^{143}Nd/^{144}Nd$ range of 0.51295–0.51358 than the Megado clinopyroxene with 0.51291–0.51367 (Fig. 7a). There is no clear difference between the Sr and Nd isotopic compositions of the clinopyroxene from the harzburgite and lherzolite. The $^{87}Sr/^{86}Sr$ and $^{143}Nd/^{144}Nd$ of clinopyroxene from harzburgite vary from 0.702964 to 0.703005 and 0.512996–0.513011, respectively, while those of clinopyroxene from the two clinopyroxenite samples are 0.70292–0.70295 and 0.512914–0.51294, respectively. The clinopyroxene from the Dillo and Megado xenoliths also shows Sr and Nd isotopic composition similar to those from the southern Ethiopian rift Mega xenoliths (Bianchini et al. 2014) but contain more radiogenic Nd and less radiogenic Sr than most xenoliths from the Assab area (Teklay et al. 2010), Ethiopian plateau and rift basalts (Kieffer et al. 2004; Shinjo et al. 2010) (Fig. 7a). The variation of $^{176}Hf/^{177}Hf$ in the clinopyroxene from the lherzolite ranges from 0.28289 to 0.28375. Some samples from Megado show higher Hf isotopic abundances than those from Dillo, which vary from 0.28289 to 0.28342. Analyses of Hf isotopes in clinopyroxene from a harzburgite

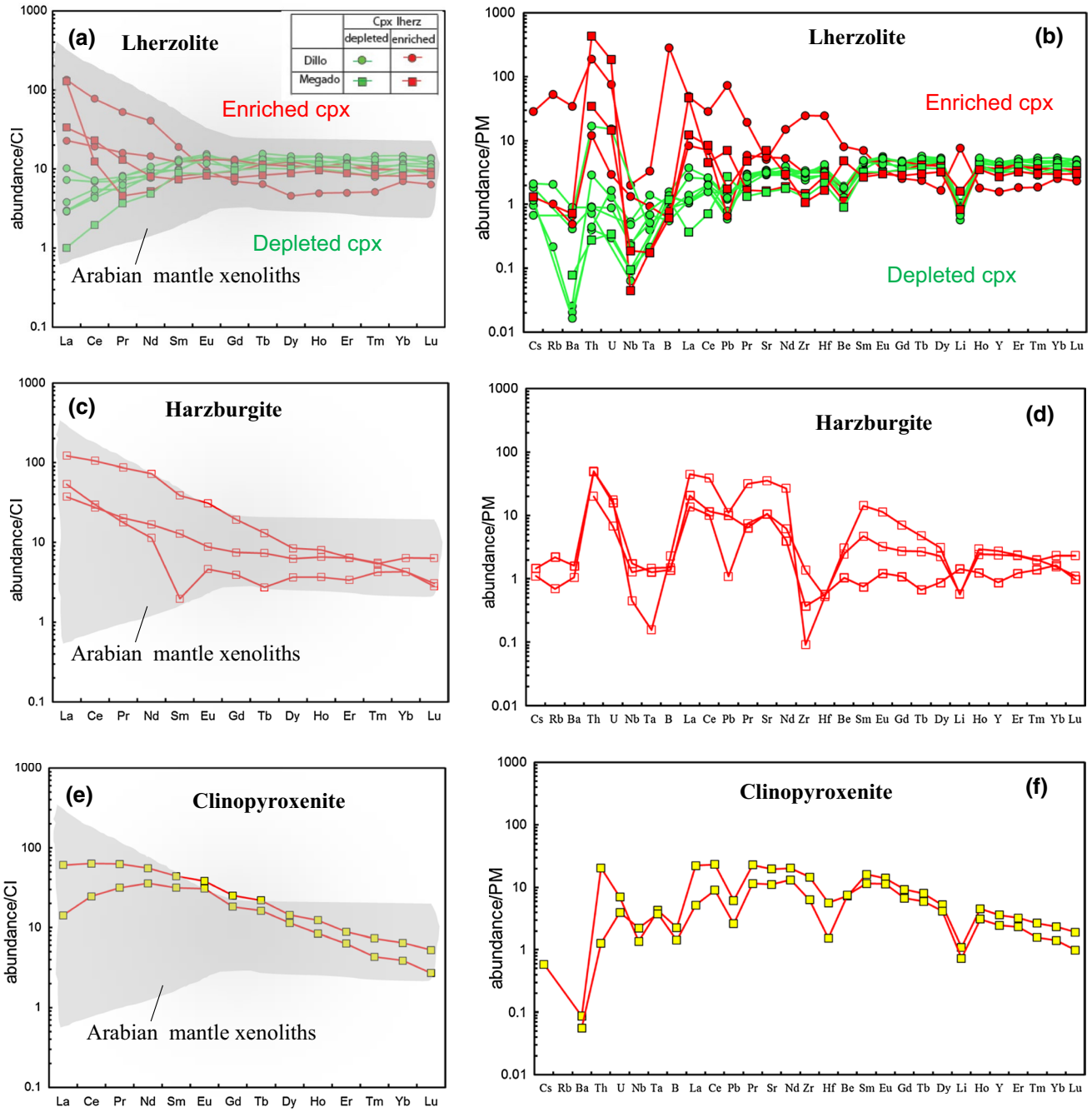

Fig. 6 Chondrite (CI) REE normalized (*left column*) and (**b**) primitive mantle (PM)-normalized (*right column*) multi-trace element variation diagrams of clinopyroxene from (**a**, **b**) Dillo and Megado lherzolites, (**c**, **d**) Megado harzburgites and (**e**, **f**) Megado clinopyroxenites. Normalizing values are from Sun and McDonough (1989) for REE and McDonough and Sun (1995) for trace elements. Data for Arabian clinopyroxene peridotites are taken from Shaw et al. (2007), Nasir and Rollinson (2009) and Nasir and Stern (2012). The lherzolite, harzburgite and clinopyroxenite in the table legend are denoted as lherz, harz and cpxt, respectively

sample and one clinopyroxenite, respectively, yielded $^{176}Hf/^{177}Hf = 0.28385$ and $^{176}Hf/^{177}Hf = 0.28301$, representing the higher and lower ends of all analyzed data, respectively. With the exception of one clinopyroxenite, $^{176}Hf/^{177}Hf$ ratios of most peridotite samples plot outside the field of MORB. Some clinopyroxene from Megado, however, has higher $^{143}Nd/^{144}Nd$ and $^{176}Hf/^{177}Hf$ than present-day DMM values (Fig. 7b).

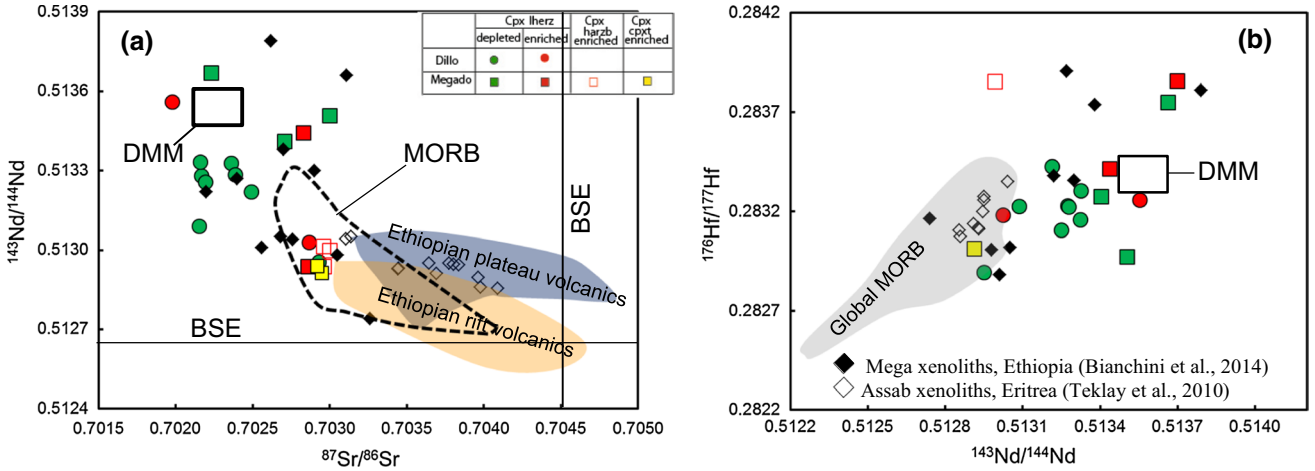

Fig. 7 Isotope variation diagrams (**a**) Sr–Nd and (**b**) Nd–Hf. Clinopyroxene data for the southern Ethiopia Mega xenoliths from Bianchini et al. (2014) and Assab xenoliths from Teklay et al. (2010), and basalts from the Ethiopian rift and plateau from Kieffer et al. (2004) and Shinjo et al. (2010) are shown for comparisons. Filled and unfilled diamond symbols are data of clinopyroxene from southern Ethiopian rift xenoliths (Bianchini et al. 2014) and clinopyroxene from Assab mantle xenoliths from Eritrea (Teklay et al. 2010). BSE and DMM denote Bulk Silicate Earth and Depleted MORB Mantle, respectively. Global MORB from PetDB (http://www.petdb.org). Circle and square symbols represent the Dillo and Megado localities, respectively

Discussion

Nature of continental lithospheric mantle

The pressure estimates generated using the orthopyroxene solvus geobarometer of MacGregor (2015) define a narrow range of equilibrating pressure from 13 to 14.4 kbar for Dillo and 9.9–13.3 kbar for Megado mantle xenoliths (Fig. 5; Supplementary Table 2). Clinopyroxenite and harzburgite from Megado give lower pressure estimates (9.9 kbar and 11.1–12.3 kbar, respectively) than the lherzolites but comparable with Mega (6.7–13 kb, Conticelli et al. 1999; 10–16 kb, Beccaluva et al. 2011), Injibara (9–13 kb; Beccaluva et al. 2011) and Assab (8–20 kb, Teklay et al. 2010) mantle peridotites. The pressure estimates obtained for lherzolites (13–14.4 kb) from both Dillo and Megado are in good agreement with previous pressure estimates for mantle peridotites from Dillo and Megado (12.8–22.2 kb, Meshesha et al. 2011) and Injibara (13–20 kb, Ferrando et al. 2008). There is no significant systematic pressure–temperature difference between the harzburgite and lherzolite units (Fig. 5), suggesting the absence of lithological layering. The East African rift xenoliths including Tanzania, Kenya and Ethiopia show variable pressure and temperature conditions (Fig. 5). The Tanzanian xenoliths usually fall near the conductive continental geothermal gradient of 40 mW/m^2 (Dawson et al. 1970 and Lee et al. 2000), while the Kenyan (Kaeser et al. 2009) and Ethiopian (Bedini et al. 1997; Rogers et al. 1999; Beccaluva et al. 2011; Meshesha et al. 2011) xenoliths represent a high geothermal gradient. Our mantle xenoliths results and those of previous studies in Ethiopia lie between 60 and 150 mW/m^2 (Fig. 5), which is not common for continental environments (40 mW/m^2; Pollack and Chapman 1977). This probably indicates the presence of upwelling mantle beneath the study area and is consistent with the active tectonic setting of the southern MER that is located very close to the Kenya plume (Shinjo et al. 2010). Trace element compositions of clinopyroxene do not show considerable variations between cores and rims, and this shows the internal homogenization of minerals by diffusion during or after magmatic processes. However, REE patterns of clinopyroxene are variable among the samples; some are LREE depleted due to melt extraction (Ottonello et al. 1984), while others are LREE enriched due to melt addition (Zhang et al. 2012). Overall, the variations in texture, major trace elements and isotopic compositions in the Dillo and Megado xenoliths indicate multiple processes modifying the CLM of the southern MER. These include (1) depletion, (2) enrichment and (3) latest melting processes as explained below.

Depletion processes

The depleted mantle xenoliths from the southern MER have major element compositions that indicate high degrees of melt extraction and are also similar to the composition of Ethiopian rift and plateau xenoliths obtained from previous studies (Ayalew et al. 2009; Beccaluva et al. 2009, 2011; Frezzotti et al. 2010; Meshesha et al. 2011; Bianchini et al. 2014; Alemayehu et al. 2016a). In the OSMA (Arai 1994; Fig. 4b), peridotites evolve from low to high Cr#, but all lherzolites from this study fall into the low Cr# and Fo

region of OSMA, implying that they are mantle-derived residual peridotite. The orthopyroxene from harzburgite has lower Al_2O_3 than that from the lherzolite, indicating depletion of Al_2O_3 by partial melting (Jaques and Green 1980). The composition of orthopyroxene from the Dillo and Megado xenoliths is identical to that of off-craton spinel peridotite xenolith suites worldwide, but is clearly distinct from on-cratonic suites (Fan et al. 2001), which is consistent with the actual tectonic setting of the area. The clinopyroxene from harzburgite contains more Cr_2O_3 than that from the lherzolite and clinopyroxenite indicating a high degree of partial melting of harzburgite, and consistent with olivine, orthopyroxene and spinel compositional variation in harzburgite.

The LREE depletion in clinopyroxene is the result of an earlier stage of melt extraction and consistent with the report of Menzies (1983). The calculated REE abundances in residues after fractional partial melting of primitive spinel lherzolite using a partition coefficient from the compilation by Ionov and Harmer (2002) and an algorithm from Johnson et al. (1990) are shown in Fig. 8a and b. The LREE and MREE abundances in lherzolites are comparable with the result of 5–15 % fractional partial melting from Ce to Lu, while the lowest HREE abundances in harzburgite and clinopyroxenite require 20–25 % of fractional partial melting from Nd to Lu. The low $^{87}Sr/^{86}Sr = 0.701982$ and the high $^{143}Nd/^{144}Nd = 0.513666$ and $^{176}Hf/^{177}Hf = 0.283424$ isotopic compositions of some of the clinopyroxene are even more depleted than present-day DMM, suggesting that a high degree of partial melting and melt extraction probably occurred around the time of Pan-African crustal formation (900–500 Ma; e.g., Stern and Kröner 1993; Stern and Abdelsalam 1998).

Enrichment processes

The interaction between LREE-enriched melt and/or fluid with peridotite can form cryptic or modal metasomatism in mantle xenoliths (Frey and Martin 1978; Harte 1977; Dawson 1984). Modal metasomatism adds new phases to an assemblage, and cryptic metasomatism affects the trace element abundances of the phases present but does not change their modal abundances. Evidence for modal metasomatism in our study is restricted to the presence of trace amounts of amphibole in the Dillo xenoliths (Meshesha et al. 2011) and sulfide minerals in the Megado xenoliths. However, cryptic metasomatism of variable type and/or extent is recorded by LREE enrichment of clinopyroxene in xenoliths from both localities. Lorand et al. (2003) found sulfides along grain boundaries of silicate minerals in Mega xenoliths from southern Ethiopia and suggested a metasomatic origin possibly associated with East Africa rift volcanism. Moreover, granular peridotites from the southern

Fig. 8 Clinopyroxene chondrite-normalized REEs. (**a**) Depleted and (**b**) enriched clinopyroxene. REE fractional melting model compared with depleted and enriched cpx. Cpx compositions for residues of 1–30 % partial melting of primitive mantle (Sun and McDonough 1989) are also shown. The REE abundances were calculated using the partition coefficients from the compilation by Ionov and Harmer (2002) and an algorithm from Johnson et al. (1990) using spinel lherzolite that contains 0.55 olivine, 0.25 orthopyroxene, 0.18 clinopyroxene and 0.02 spinel. The REE patterns of LREE-enriched cpx and calculated silicate melt for (**c**) lherzolite (**d**) harzburgite and clinopyroxenite. Chondrite-normalized values are from Sun and McDonough (1989). Southern Ethiopian rift basalts (Shinjo et al. 2010) are used for evaluation of metasomatic agent and represented by solid black lines. *Dashed lines* denote calculated melt in equilibrium with enriched cpx. Hypothetical silicate melts in equilibrium with those of cpx were calculated using clinopyroxene–melt partition coefficients from Kelemen and Dick (1995). (**e**) Ti/Eu versus $(La/Yb)_N$ for cpx in mantle xenoliths compared with Ethiopian rift xenoliths (Bedini et al. 1997; Rogers et al. 1999; Bedini and Bodinier 1999; Conticelli et al. 1999; Lorand et al. 2003; Beccaluva et al. 2009; Meshesha et al. 2011; Bianchini et al. 2014). Carbonatite and silicate metasomatism fields are from Yaxley et al. (1991), Rudnick et al. (1993), Coltorti et al. (1999)

Ethiopia region of the Mega area indicate the presence of large-scale metasomatism of the CLM with basaltic melt that caused the depletion of the platinum group elements (PGE) without significant Pd/Ir enrichment, even though the percolating melt precipitated sulfides in addition to metasomatic non-sulfide minerals like clinopyroxene (Lorand et al. 2003 and reference therein). Similarly, sulfide inclusions occurring in different habits and related to metasomatic events have been described in mantle xenoliths from many localities including West Eifel, Germany (Shaw 1997), Allyn River, eastern Australia (Powell and O'Reilly 2007), Tenerife, Canary Islands (Frezzotti et al. 2002), Kerguelen Islands, Southern Indian Ocean Spitsbergen (Amundsen et al. 1987), and Mega, southern Ethiopia (Reisberg et al. 2004).

The REE melt compositions in equilibrium with clinopyroxene have been calculated for the enriched samples to compare the metasomatic agents involved in the enrichment processes with the southern Ethiopian rift volcanic rocks (Fig. 8c, d). Calculated mafic silicate melts in equilibrium with enriched clinopyroxene have slightly different chondrite-normalized REE patterns to the southern Ethiopian rift volcanic rocks. In particular, the calculated melts are highly enriched in La and Ce and depleted in MREE and HREE, whereas the rifts volcanic has elevated HREE (Fig. 8a, b). Thus, a mafic silicate melt similar to the Ethiopian rift volcanic rocks is unlikely to be the metasomatic agent responsible for the enriched clinopyroxene of lherzolite, harzburgite and clinopyroxenite. Asthenospheric melt formed at a relatively low degree of partial melting during the East African rift development could possibly be the metasomatic agent for these areas, consistent with Rogers et al. (1999) and Beccaluva et al. (2011).

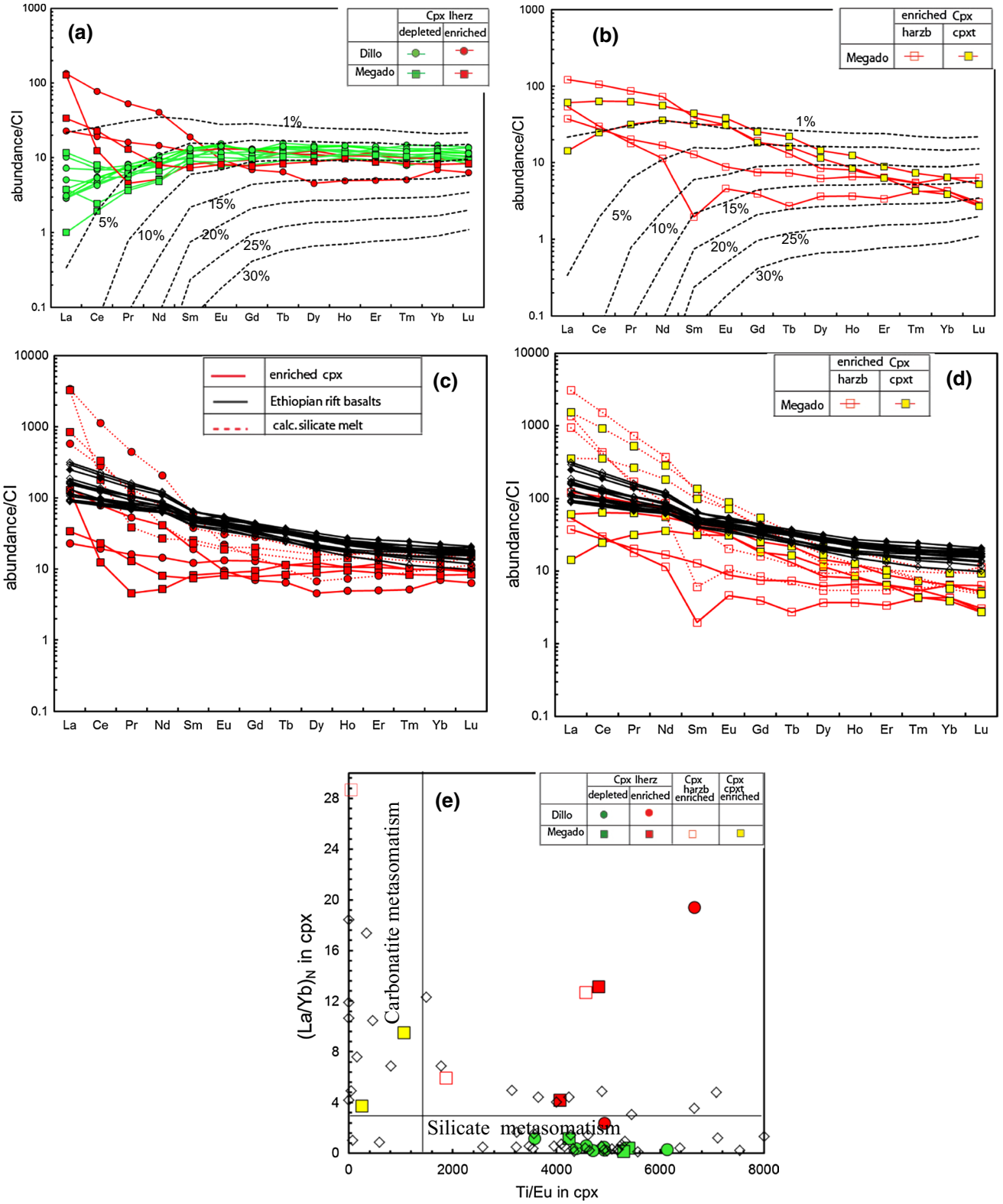

The Ti/Eu versus $(La/Yb)_N$ discrimination diagram (Fig. 8e) is useful for understanding the type and nature of the metasomatic agent(s) (Yaxley et al. 1991; Rudnick et al. 1993; Coltorti et al. 1999). The two clinopyroxenites and one harzburgite samples have high $(La/Yb)_N$ and low Ti/Eu, implying that the metasomatic agent was carbonatite-rich melt (Fig. 8e). Only one lherzolite sample is consistent with silicate metasomatism, while the other lherzolite

and two harzburgite samples represent high $(La/Yb)_N$ and Ti/Eu possibly indicating the effect of both silicate–carbonatite metasomism or overprinting by multiple episodes of metasomatism (Coltorti et al. 1999). Similarly, previous studies on the southern Ethiopia xenoliths from the Mega area (Bedini et al. 1997) indicate both carbonatite and silicate metasomatism occurring on a kilometer scale, involving gradual solidification of melt infiltrated into the lithospheric mantle through successive melt–rock reactions down a conductive, thermal gradient (reference therein). This process is associated with a strong chemical evolution of the melt, from an original basaltic composition to progressively volatile-enriched compositions, culminating in low-T, small volume of carbonatite melts. The presence of carbonatite-peridotite interaction is usually identified by enrichment in REEs without enrichment in high field strength elements (Hauri et al. 1993). The enriched samples in this study do not show enrichment in high field strength elements (Zr, Hf, Ta and Nb) (Fig. 6b, d, f), supporting the effect of carbonatite metasomatism. Thus, we suggest that the metasomatic agents for Dillo and Megado xenoliths have combined characteristics of carbonatite and silicate melt, consistent with previous studies from southern Ethiopia of Mega xenoliths (Bedini et al. 1997).

There is no systematic difference in Sr and Nd isotopic compositions between the depleted and enriched clinopyroxene from the lherzolites. The enriched clinopyroxene from lherzolites is characterized by high $^{176}Hf/^{177}Hf$ and high $^{143}Nd/^{144}Nd$ (Nd–Hf coupling), suggesting the effect of a small volume of melt that only changed trace element composition but not the isotopes. The enriched clinopyroxene from the Megado harzburgite has high $^{176}Hf/^{177}Hf$ at relatively low $^{143}Nd/^{144}Nd$ (Nd–Hf decoupling) suggesting the resistance of Hf isotopes to large volume of metasomatic melt compared with Nd isotopes. Clinopyroxene from the Megado clinopyroxenite has relatively lower Nd–Hf and similar Sr isotopic compositions compared with that from the lherzolite and harzburgite. This implies that the melt that influenced the Megado clinopyroxenite was probably characterized by low Sr–Nd–Hf isotopic compositions. The clinopyroxenite might also be the product of melt–harzburgite interaction at large melt/peridotite ratios. The presence of sulfide minerals in the harzburgite and clinopyroxenite as well as their similarity in REE pattern, and Sr and Nd isotopic compositions, could also suggest a genetic similarity between the harzburgite and clinopyroxenite xenoliths. The insignificant influence of Pan-African subducting materials has already been confirmed by the low $^{87}Sr/^{86}Sr$ ratios of the clinopyroxene, strengthening the case that the asthenospheric melt from depleted asthenosphere that does not contain enriched (subduction) components may be the best metasomatic candidate in the study area. Largely, geochemical and isotopic data reveal the presence of extensive interaction between the depleted CLM and asthenospheric derived melts.

Latest melting processes

Several studies have been conducted worldwide to investigate the occurrence and genesis of spongy texture in mantle xenoliths (Carpenter et al. 2002; Norman 1998; Su et al. 2011). Spongy textures occur in both the depleted and enriched groups of the Megado and Dillo xenoliths and are evidence of distinct latest melting processes responsible for the formation of the porous or sieve-like spongy texture. The latest decompressional partial melting facilitated by the melt-/fluid-type-induced metasomatism could be responsible for the formation of this texture (Carpenter et al. 2002; Su et al. 2011; Fig. 2g, h). The spongy texture has no relation with depth, xenolith types or composition, and is distributed throughout the CLM, indicating that melt- and/or fluid-induced metasomatism has affected the entire CLM of southern Ethiopia. This indicates the occurrence of large-scale mantle upwelling, which probably occurred very close to the ejection period of the xenoliths to the surface and extended throughout the whole southern Ethiopia rift. Moreover, from the major trace element abundance, the lack of systematic differences between the spongy and normal clinopyroxene suggests that such compositional differences cannot be produced during the latest melting processes among the clinopyroxene. Glass in the spongy clinopyroxene represents a breakdown product of clinopyroxene by heating from the host rock during ascent, combined with decompression and incongruent partial melting of clinopyroxene in a closed system, or reaction at low melt/rock ratio (Ionov and Hofmann 1994 and reference therein). This is consistent with our observation. Thus, post-rifting and active plume impingement of the EARS have produced widespread metasomatic disequilibrium textures like the spongy texture, reflecting ongoing processes, and this is consistent with the current active tectonic setting of the study area.

Timing of melt extraction

The Pan-African crust (900–500 Ma) usually has a radiogenic Nd and Hf isotopic composition that varies from εNd(t) 6.6–7.7 and εHf(t) 10.9–15.5 (e.g., Stern and Kröner 1993; Stern and Abdelsalam 1998; Vervoort and Blichert-Toft 1999). In southern Arabia around Yemen, relatively older Early Proterozoic to Late Archean crust (1.7–2.9 Ga) has been reported (Windley et al. 1996), and the genesis of Oligocene flood and intraplate volcanism in Yemen was associated with an Archean crustal component (Baker et al. 1996). There is also evidence for the presence of Archean lithospheric mantle beneath the southern MER (Reisberg

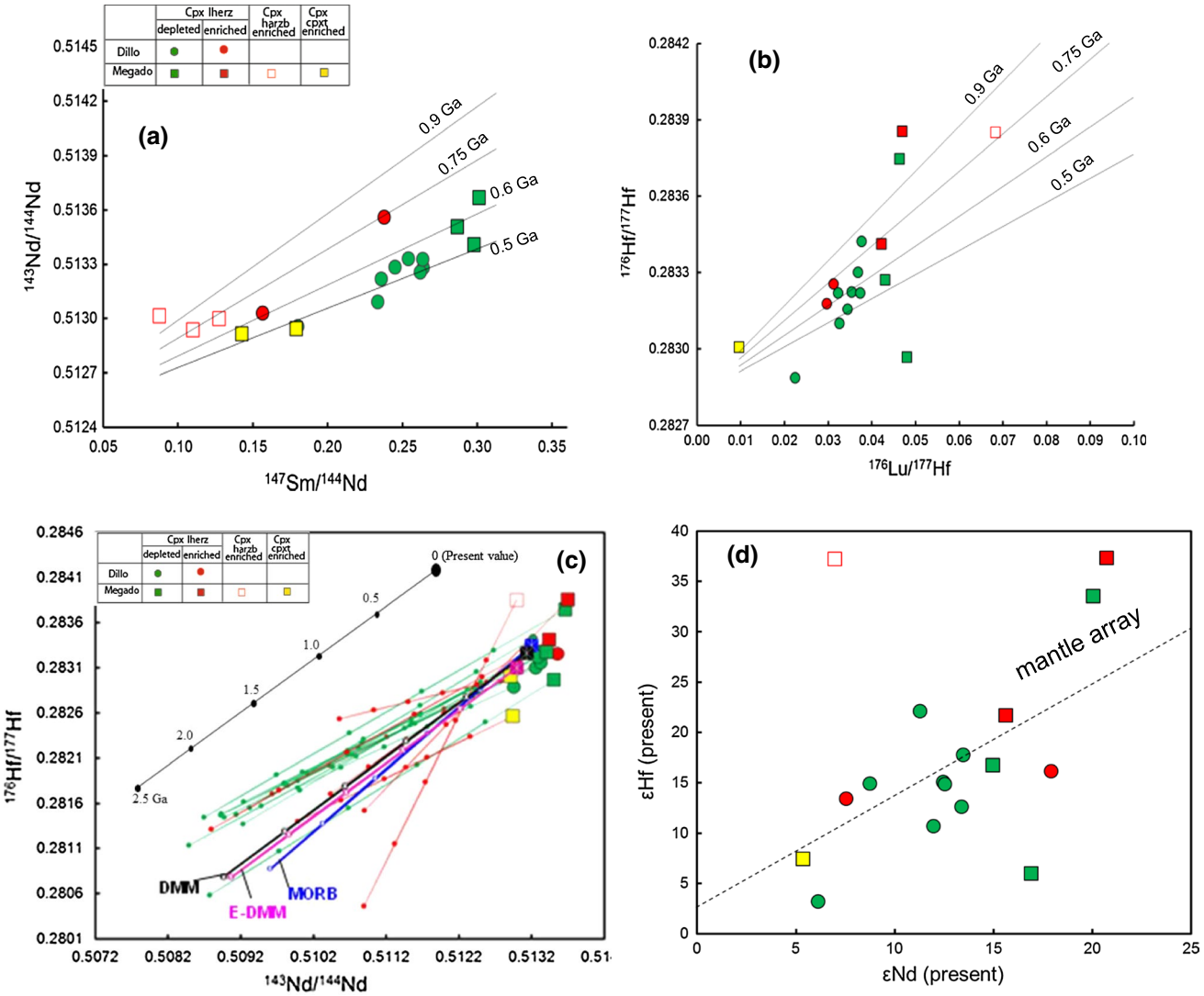

Fig. 9 (**a**) $^{147}Sm/^{144}Nd$ versus $^{143}Nd/^{144}Nd$ and (**b**) $^{176}Lu/^{177}Hf$ versus $^{176}Hf/^{177}Hf$ isochron evolution diagram for depleted- and enriched clinopyroxene compared with reference isochron at different ages taking into account the maximum (0.9 Ga) and minimum (0.5 Ga) age of the Pan-Africa orogen (Stern and Kröner 1993; Stern and Goldstein 1996; Stern and Abdelsalam 1998). The parameters used to calculate the reference isochrons are as follows: $^{143}Nd/^{144}Nd_{CHUR,present} = 0.512637$ s; $^{147}Sm/^{144}Nd_{CHUR,present} = 0.1964$; $\lambda^{147} = 6.539 \times 10^{-12}$/year (Goldstein et al. 1984); $^{176}Hf/^{177}Hf_{CHUR,present} = 0.282785$; $^{176}Lu/^{177}Hf_{CHUR,present} = 0.0336$; $\lambda^{176} = 1.94 \times 10^{-11}$/year (Vervoort et al. 1999). (**c**) $^{143}Nd/^{144}Nd$ versus $^{176}Hf/^{177}Hf$ isotope evolution diagram for depleted and enriched clinopyroxene. Large symbols are present isotopic values. The small circle marked at 0.5-Ga intervals on the lines represents initial isotopic values at 0.5, 1, 1.5, 2 and 2.5 Ga to estimate the xenoliths source. The DMM, E-DMM and MORB (Handler et al. 2005) are shown for comparison. (**d**) εNd versus εHf diagram for clinopyroxene separates Dillo from Megado xenoliths. Mantle array after Nowell et al. (1998)

et al. 2004). The Re depletion age of the most depleted mantle xenoliths from southern Ethiopia in the Mega area indicates that melt extraction occurred between 2.4 and 2.8 Ga, which is older than the overlying Pan-African crust. This suggests a major decoupling between the crust and the lithospheric mantle (Reisberg et al. 2004) in the region. However, most of the mantle xenoliths from Dillo and Megado fall between 900 and 500 Ma on Sm–Nd and Lu–Hf reference isochrons (Fig. 9a, b) consistent with the age range of Pan-African orogeny. Therefore, the age of melt extraction for the Dillo and Megado CLM could be the same as that associated with Pan-African crustal formation (900–500 Ma) (e.g., Stern and Kröner 1993; Stern and Abdelsalam 1998; Vervoort and Blichert-Toft 1999; Stern and Johnson 2010). The initial Nd and Hf isotopic ratios were calculated at 0.5, 1, 1.5, 2 and 2.5 Ga plot away from the trend defined by MORB, DMM and E-DMM between the ages of 0.9–2.8 Ga of previous studies determined from southern Ethiopian peridotites (Reisberg et al. 2004; Meshesha et al. 2011; Bianchini et al. 2014), indicating that

the Dillo and Megado xenoliths could have been produced by melt extraction from the asthenosphere during Pan-African orogenesis (Fig. 9c). As suggested by previous studies (Orlando et al. 2006; Meshesha et al. 2011) and this study, depletion of the CLM beneath the southern Ethiopia rift most likely occurred close to the time of Pan-African crust formation (Stern and Goldstein 1996; Stern and Abdelsalam 1998). This implies that the CLM of the Dillo and Megado areas was formed at a time similar to the formation of the overlying crust. However, there is no applicable method to define the absolute ages of the metasomatic events. Nevertheless, the maximum and minimum ages could be correlated with Pan-African Orogeny and Cenozoic rifting of the EARS, respectively, where the former might be responsible for amphibole and sulfide formation and the latter could have produced the signature of LREE enrichment signatures in the clinopyroxene.

Heterogeneity of the continental lithospheric mantle

Petrographical observation, and major trace element and isotopic composition studies suggest that the evolution of the southern Ethiopia rift is more or less similar to those of other Ethiopian plateau and rift CLM and are refractory to fertile in composition (Alemayehu et al. 2010; Meshesha et al. 2011; Bianchini et al. 2014). Mineralogically, similar to the plateau, southern rift xenoliths contain amphiboles (Orlando et al. 2006; Meshesha et al. 2011), but amphiboles were not observed in this study. Moreover, the Dillo and Megado xenoliths are usually rich in clinopyroxene (lherzolites), with some of them being clinopyroxenite. These observations, together with previous studies, indicate that the high fertility of the CLM of southern MER is similar to the CLM beneath the Arabian plate (McGuire 1988; Henjes-Kunst et al. 1990; Nasir and Rollinson 2009; Nasir and Stern 2012). The harzburgite samples are characterized by high Cr_2O_3 and Mg# in olivine and pyroxenes, suggesting the presence of refractory CLM beneath the study area. However, this refractory nature is clearly different from kimberlite-hosted mantle xenoliths from Archean cratons (Boyd 1998; Griffin et al. 1998; Fig. 4a). The Fo contents of olivine in the lherzolite and harzburgite are mostly <91, representing cratonic fertile mantle (Zheng et al. 2007). Thus, the prevalence of fertile peridotite xenoliths from Dillo and Megado indicates that the CLM replacement and/or formation beneath the southern Ethiopian rift most likely occurred post-Archean, and it is different from the CLM of the Tanzanian craton peridotite whose harzburgites have olivine Fo > 92 and are interpreted as relics of the Archean cratonic mantle (Lee et al. 2000; Rudnick et al. 2004). The isotope systematics of Re–Os from sulfide and Lu–Hf and Sm–Nd from clinopyroxene, combined with the tectonic setting of the area, suggests that Proterozoic–Phanerozoic lithospheric thinning and mantle replacement was heterogeneously distributed across the southern Ethiopian rift in space and time (Lorand et al. 2003; Reisberg et al. 2004; Meshesha et al. 2011; Bianchini et al. 2014). The lateral spreading of the lithosphere, accompanied by asthenospheric upwelling and melt-peridotite interaction, is the most probable mechanism for the lithospheric fertilization as well as compositional heterogeneities beneath the Arabian plate (Henjes-Kunst et al. 1990; Nasir and Rollinson 2009; Nasir and stern 2012). A similar interpretation could explain the CLM of the southern Ethiopia rift zone. Textures and major trace element abundances of spinel mantle xenoliths from the southern Ethiopian rift show that the CLM beneath this tectonic zone is texturally and compositionally heterogeneous on the scale of <100 km. The very high radiogenic values (εHf up to +1076) of the Mega clinopyroxene suggest that the present-day MER lithospheric mantle domains underwent melting, possibly in the presence of residual garnet, billions of years ago, thereby fractionating the Lu/Hf ratio and ultimately leading to extremely high $^{176}Hf/^{177}Hf$ (Bianchini et al. 2014 and reference therein).

Considering the maximum and the minimum age of Pan-African orogeny (e.g., Stern and Kröner 1993; Stern and Abdelsalam 1998; Vervoort and Blichert-Toft 1999), 0.9, 0.75, 0.6 and 0.5 Ga reference isochrons are illustrated on a $^{147}Sm/^{144}Nd$ versus $^{143}Nd/^{144}Nd$ and $^{176}Lu/^{177}Hf$ versus $^{176}Hf/^{177}Hf$ diagram (Fig. 9a, b). However, neither the depleted nor the enriched clinopyroxene defined a trend. The scattered data for the enriched samples could be due to metasomatism, while those for the depleted clinopyroxene may be ascribed to preexisting mantle heterogeneity before and/or during Pan-Africa orogeny, as a result of which εNd and εHf are both higher and lower than the depleted mantle. Although such extreme Nd and Hf isotope heterogeneity is not observed today (present-day εNd = 6.14–13.5 for Dillo and 15–20.1 for Megado), the wide range of εHf values (3.13–22.1 for Dillo and 5.93–33.5 for Megado) (Fig. 9d) for the depleted clinopyroxene illustrates the extent of isotopic heterogeneity that existed in the southern Ethiopia CLM prior to metasomatism.

Conclusions

Mantle xenoliths from the southern main EAR mostly show either protogranular or porphyroclastic textures, with some displaying spongy texture. Their major trace element variations are within the range of existing Ethiopian mantle xenolith data. Trace element compositions in particular show large geochemical heterogeneity, with LREE-depleted and LREE-enriched patterns, and other variable trace element distributions. Three major processes

have dominantly influenced the CLM beneath the southern MER: (1) major depletion related to partial melting and melt extraction, which gave rise to strong variations in major oxides and trace elements and produced radiogenic Nd–Hf at relatively low Sr isotopic compositions, (2) multistage metasomatism as evidenced by the presence of sulfide minerals and variable enrichment of incompatible elements, with enrichment due to involvement of an asthenospheric melt, and (3) the latest melting process, which is independent of the geochemical composition and identified by spongy texture—it might be related to post-rifting and active plume impingement beneath the EARS, resulting in widespread metasomatic disequilibrium textures. Most of the investigated samples are between 900 and 500 Ma on Sm–Nd and Lu–Hf reference isochrons, within the age range of Pan-African orogenesis. Initial Nd and Hf isotopic compositions calculated at 0.5, 1, 1.5, 2 and 2.5 Ga plot away from the trend of various types of MORBs between the ages of 0.9–2.8 Ga of previous studies determined from southern Ethiopia peridotites, probably indicating that the xenoliths could have been produced by melt extraction from the asthenospheric mantle. There is no significant difference in $^{87}Sr/^{86}Sr$ ratios between the depleted and enriched clinopyroxene, suggesting that the metasomatising agent(s) were mainly derived from the asthenospheric mantle. Generally, the mineralogical and isotopic compositions of the xenoliths show heterogeneity of the CLM beneath the southern Ethiopia rift zone. Such heterogeneity could have resulted from various degrees of melt extraction of the CLM and metasomatism by melts from the asthenospheric mantle.

Acknowledgments MA highly acknowledges the grant obtained from the Chinese Academy of Sciences for postdoctoral fellowship for developing countries (Grant No. 2014FFBZ003). We would like to appreciate Mr. Qian Mao, Mr. Yu-Guang Ma and Dr. Zhu Bin for their assistance in major element analysis using EMPA. Dr. Yue-Heng Yang and Dr. Yan Xiao are thanked for their assistance in trace element determination using LA-ICP-MS. Dr. Yue-Heng Yang and Mr. Li Yang are greatly appreciated for Rb, Sr, Sm, Nd, Lu and Hf elemental separation in the ultra-clean laboratory and Lu–Hf isotope analyses using MC-ICP-MS. Dr. Zhu-Yin Chu and Miss Wang Xiuli are also appreciated for Rb–Sr and Sm–Nd isotope analysis using TIMS. Prof. Yan-Jie Tang, Prof. Tyrone Rooney and Prof. Bishal Nath Upreti are thanked for giving detailed scientific comments and English correction on an earlier version of this manuscript. Dr. Reitz Meredith and Dr. Greig A. Paterson are also appreciated for English language correction on the on the first and second revised version of this manuscript. The authors also extend their appreciation to Geological Survey of Ethiopia for providing materials related to the study area. Our appreciation also goes to Addis Ababa Science and Technology University, School of Earth Science and Mining Engineering, University of Gondar and Arba Minch University Earth Science department for fieldwork material support. The fast careful detail editorial handling and comments from Chief Editor Prof. Wolf-Christian Dullo and Associate Editor Prof. Victoria Pease are highly appreciated. We gratefully acknowledge the two reviewers, Dr. Katie Smart and Dr. Bernard Bonin, for their numerous constructive suggestions and comments that greatly improved this paper. This research work has also benefited from the financial support from the National Science Foundation of China to Melesse Alemayehu (Grant No. 41450110429) and Hong-Fu Zhang (Grant No. 91414301).

References

Abdelsalam M, Stern R (1996) Sutures and shear zones in the Arabian-Nubian Shield. J Afr Earth Sci 23:289–310

Alemayehu M (2010) Nature and evolution of northwestern and southern Ethiopian sub-continental lithospheric mantle: implication from petrology, geochemistry, and geochronology of mantle xenoliths. PhD thesis Okayama Univ, Japan

Alemayehu M, Tak K, Ota T, Ryoji T, Moriguti T, Nakamura E (2010) Sr–Nd–Hf–Pb isotopic characteristics of Northwestern and southern Ethiopian lithospheric mantle. Geochim Cosmochim Acta 74:A697

Alemayehu M, Zhang HF, Tang Y, Xiao Y, Abraham S, Haji M (2015) Geochemical evolution of sub-continental lithospheric mantle of Ethiopian plateau and rift zone. Goldschmidt conference 2015 Abstract # 2098

Alemayehu M, Zhang HF, Zhu B, Fentie B, Abraham A, Haji M (2016a) Petrological constraints on evolution of continental lithospheric mantle beneath the northwestern Ethiopian plateau: insight from mantle xenoliths from the Gundeweyn area, East Gojam, Ethiopia. Lithos 240–243:295–308

Alemayehu A, Zhang HF, Zhu B, Tang Y, Meten M, Getahun E, Haji M (2016b) Multistage evolution of sub-continental lithospheric mantle beneath Ethiopian plateau and rift. Goldschmidt conference 2016 Abstract accepted

Alemayehu M, Hong-Fu, Zhang HF, Aulbach S (2016c) Evaluation of mantle processes in an extensional regime: Insight from in situ O and Sr isotope systematics of mantle xenoliths from Ethiopia. J Geol accepted

Amundsen HEF, Griffin WL, O'Reilly SY (1987) The lower crust and upper mantle beneath northwestern Spitsbergen: evidence from xenoliths and geophysics. Tectonophysics 139:169–185

Arai S (1994) Characterization of spinel peridotite by olivine-spinel compositional relationships: review and interpretation. Chem Geol 113:191–204

Ayalew D, Yirgu G, Ketefo E, Barbey P, Ludden J (2003) Intrusive equivalents of food volcanics: evidence from petrology of xenoliths in Quaternary Tana basanites Ethiopia. Ethiop J Sci 26:93–102

Ayalew D, Arndt N, Bastien F, Yirgu G, Kieffer B (2009) A new mantle xenolith locality from Simien shield volcano, NW Ethiopia. Geol Mag 146:144–149

Baker J, Thirlwall M, Menzies M (1996) Sr–Nd–Pb isotopic and trace element evidence for crustal contamination of plume derived flood basalts; Oligocene flood volcanism in western Yemen. Geochim Cosmochim Acta 60:2559–2581

Beccaluva L, Bianchini G, Natali C, Siena F (2009) Continental flood basalts and mantle plumes: a case study of the northern Ethiopian plateau. J Petrol 50:1377–1403

Beccaluva L, Bianchini G, Ellam RM, Natali C, Santato A, Siena F, Stuart FM (2011) Peridotite xenoliths from Ethiopia: inferences on mantle processes from plume to rift settings. Geol Soc Am Spec Pap 478:77–104

Bedini RM, Bodinier JL (1999) Distribution of incompatible trace elements between the constituents of spinel peridotite xenoliths: ICP-MS data from the East African Rift. Geochim Cosmochim Acta 63:3883–3900

Bedini RM, Bodinier JL, Dautria JM, Morten L (1997) Evolution of LILE enriched small melt fractions in the lithospheric mantle:

a case study from the East African Rift. Earth Planet Sci Lett 153:67–83

Bianchini G, Julia G, Bryce JG, Blichert-Toft J, Beccaluva L, Natali C (2014) Mantle dynamics and secular variations beneath the East African Rift: insights from peridotite xenoliths (Mega, Ethiopia). Chem Geol 386:49–58

Boyd F (1998) The origin of cratonic peridotites: a major-element approach. Int Geol Rev 40:755–764

Brey GP, Kohler T (1990) Geothermobarometry in four-phase lherzolites II; new thermo barometers and practical assessment of existing thermobrometers. J Petrol 31:1353–1378

Carpenter RI, Edgar AD, Thibault Y (2002) Origin of spongy textures in clinopyroxene and spinel from mantle xenoliths, Hessian Depression, Germany. Contrib Mineral Petrol 74:149–162

Chen L, Liu Y, Hu Z, Gao S, Zong K, Chen H (2011) Accurate determinations of fifty four major and trace elements in carbonate by LA-ICP-MS using normalization strategy of bulk components as 100%. Chem Geol 284:283–295

Coltorti M, Bonadiman C, Hinton RW, Siena F, Upton BGJ (1999) Carbonatite metasomatism of the oceanic upper mantle: evidence from clinopyroxenes and glasses in ultramafic xenoliths of Grande Comore, Indian Ocean. J Petrol 40:133–165

Conticelli S, Sintoni MF, Abebe T, Mazzarini F, Manetti P (1999) Petrology and geochemistry of ultramafic xenoliths and host lavas from Ethiopian volcanic province; an insight into the upper mantle under Eastern Africa. Acta Vulcanol 11:143–151

Courtillot V, Davaille A, Besse J, Stock J (2003) Three distinct types of hot spots in the Earth's mantle. Earth Planet Sci Lett 205:295–308

Davidson A (1983) The Omo river project: reconnaissance geology and geochemistry of parts of Ilubabor, Kefa, Gem-Gofa, and Sidamo, Ethiopia. Ethiop Inst Geol Surv Bull 3:89

Davidson A, Rex DC (1980) Age of volcanism and rifting in South-Western Ethiopia. Nature 283:657–658

Dawson JB (1984) Contrasting types of upper mantle metasomatism? In: Kornprobst J (ed) Kimberlites II, vol 11. Elsevier, Amsterdam, pp 519–548

Dawson JB, Powell DG, Reid AM (1970) Ultrabasic xenoliths and lava from the Lashaine Volcano, northern Tanzania. J Petrol 11:519–548

Ebinger CJ, Yemane T, Weldable G, Agonising JL, Walter RC (1993) Late eocene-recent volcanism and faulting in the southern Main Ethiopian Rift. J Geol Soc Lond 50:99–108

Fan WM, Zhang HF, Baker J, Jarvis KE, Mason PRD, Menzies MA (2001) On and off the North China craton: where is the Archean keel? J Petrol 41:933–950

Ferrando S, Frezzotti ML, Neumann ER, Astis DG, Peccerillo A, Dereje A, Gezahegn Y, Teklewold A (2008) Composition and thermal structure of the lithosphere beneath the Ethiopian plateau: evidence from mantle xenoliths in basanites, Injibara, Lake Tana Province. Mineral Petrol 93:47–78

Frey F, Martin PM (1978) Ultramafic inclusions from San Carlos, Arizona: petrologic and geochemical data bearing on their petrogenesis. Earth Planet Sci Lett 38:129–176

Frezzotti ML, Andersen T, Neumann ER, Simonsen SL (2002) Carbonatite melt-CO2 fluid inclusions in mantle xenoliths from Tenerife, Canary Islands: a story of trapping, immiscibility and fluid–rock interaction in the upper mantle. Lithos 64:77–96

Frezzotti ML, Ferrando S, Peccerillo A, Petrelli M, Tecce F, Perucchi A (2010) Chlorine-rich metasomatic H_2O-CO_2 fluids in amphibole-bearing peridotites from Injibara (Lake Tana region, Ethiopian plateau): nature and evolution of volatiles in the mantle of a region of continental flood basalts. Geochim Cosmochim Acta 74:3023–3039

Furman T, Kaleta K, Bryce J, Hanan BB (2006) Tertiary mafic lavas of Turkana, Kenya: constraints on East African plume structure and the occurrence of high-micro volcanism in Africa. J Petrol 47:1221–1244

Goldstein S, O'Nions R, Hamilton P (1984) A Sm–Nd isotopic study of atmospheric dusts and particulates from major river systems. Earth Planet Sci Lett 70:221–236

Griffin WL, O'Reilly SY, Ryan CG (1998) The composition and origin of sub-continental lithospheric mantle. In: Fei Y, Berka CM, Mysen BO (eds) Mantle petrology: field observations and high-pressure experimentation: a tribute to Francis R (Joe) Boyd, vol 6. Geochem Soc Spec Publ, pp 13–45

Handler MR, Bennett VC, Carlson RW (2005) Nd, Sr and Os isotope systematics in young, fertile spinel peridotite xenoliths from northern Queensland, Australia: a unique view of depleted MORB mantle? Geochim Cosmochim Acta 69:5747–5763

Harte B (1977) Rock nomenclature with particular relation to deformation and recrystallization textures in olivine-bearing xenoliths. J Geol 85:279–288

Hauri EH, Shimizu N, Dieu JJ, Hart SR (1993) Evidence for hot spot-related carbonatite metasomatism in oceanic upper mantle. Nature 365:221–227

Henjes-Kunst F, Altherr R, Baumann A (1990) Evolution and composition of the lithospheric mantle underneath the western Arabian Peninsula: constraints from Sr–Nd isotope systematics of mantle xenoliths. Contrib Mineral Petrol 105:406–427

Ionov DA, Harmer RE (2002) Trace element distribution in calcite-dolomite carbonatites from Spitskop: inuences for differentiation of carbonatite magmas and the origin of carbonates in mantle xenoliths. Earth Planet Sci Lett 198:495–510

Ionov DA, Hofmann AW (1994) Metasomatism induced melting in mantle xenoliths from Mongolia. J Petrol 35:753–785

Jaques AL, Green DH (1980) Anhydrous melting peridotite at 10–15 kb pressure and the genesis of tholeiitic basalts. Contrib Mineral Petrol 73:287–310

Johnson K, Dick H, Shimizu N (1990) Melting in the oceanic upper mantle: an ion microprobe study of diopsides in abyssal peridotites. J Geophys Res 95:266–2678

Kaeser B, Olker B, Kalt A, Altherr R, Pettke T (2009) Pyroxenite xenoliths from Marsabit (northern Kenya): evidence for different magmatic events in the lithospheric mantle and interaction between peridotite and pyroxenite. Contrib Mineral Petrol 157:453–472

Kampunzu AB, Mohr P (1991) Magmatic evolution and petrogenesis in the East African Rift system. In: Kampunzu AB, Lubala RT (eds) Magmatism in extensional structural settings. Springer, Berlin Heidelberg New York, pp 85–136

Kelemen PB, Dick JB (1995) Focused melt flow and localized deformation in the upper mantle; juxtaposition of replacive dunite and ductile shear zones in the Josephine peridotite, SW Oregon. J Geophys Res 100:423–438

Kieffer B, Arndt N, Lapierre H, Bastien F, Bosch D, Pecher A, Yirgu G, Ayalew D, Weis D, Jerram DA, Keller F, Meugniot C (2004) Flood and shield basalts from Ethiopia: magmas from the African superswell. J Petrol 45:793–834

Le Fevre B, Pin C (2001) An extraction chromatography method for Hf separation prior to isotopic analysis using multiple collection ICP-mass spectrometry. Anal Chem 73:2453–2460

Lee C-T, Rudnick RL (1999) Compositionally stratified cratonic lithosphere: petrology and geochemistry of peridotite xenoliths from the Labait volcano, Tanzania. In: Gurney JJ, Gurney JL, Pascoe MD, Richardson SR (eds) The PH Nixon Volume. Proceedings 7th international Kimberlite conference, Red Roof Design Cape Town, pp 503–521

Lee C, Rudnick R, McDonough W, Horn I (2000) Petrologic and geochemical investigation of carbonates in peridotite xenoliths from northeastern Tanzania. Contrib Mineral Petrol 139:470–484

Li CF, Chen FK, Li XH (2007) Precise isotopic measurements of subnanogram Nd of standard reference material by thermal ionization mass spectrometry using the NdO+ technique. Int J Mass Spectrom 266:34–41

Li CF, Li XH, Li QL, Guoa JH, Li XH, Yanga YH (2012) Rapid and precise determination of Sr and Nd isotopic ratios in geological samples from the same filament loading by thermal ionization mass spectrometry employing a single-step separation scheme. Anal Chim Acta 727:54–60

Liu YS, Hu ZC, Gao S, Günther D, Xu J, Gao CG, Chen HH (2008) In-situ analysis of major and trace elements of anhydrous minerals by LA-ICP-MS without applying an internal standard. Chem Geol 257:34–43

Lorand JP, Reisberg L, Bedini RM, Horan MF, Brandon AD, Neal CR (2003) Platinum-group elements and melt percolation processes in Sidamo spinel peridotite xenoliths, Ethiopia, East African Rift. Chem Geol 196:57–75

MacGregor ID (2015a) Empirical geothermometers and geothermobarometers for spinel peridotite phase assemblages. Int Geol Rev 57(15):1940–1974

MacGregor ID (2015–2016) Corrigendum. Int Geol Rev doi:10.1080/00206814.2015.1129752

McDonough WF, Sun SS (1995) The composition of the Earth. Chem Geol 120:223–253

McGuire AV (1988) Petrology of mantle xenoliths from Harrat al Kishb: the mantle beneath Western Saudi Arabia. J Petrol 29:73–92

Menzies MA (1983) Mantle ultramafic xenoliths in alkaline magmas: evidence for mantle heterogeneity modified by magmatic activity. In: Hawkesworth CJ, Norry MJ (eds) Continental basalts and mantle xenoliths, vol 1. Shiva Publishing, Nantwich Cheshire, pp 92–110

Mercier JCC, Nicolas A (1975) Textures and fabrics of upper mantle peridotites as illustrated by basalt xenoliths. J Petrol 16:454–487

Merla G, Abbate E, Azzaroli A, Bruni P, Canuti P, Fazzuoli M, Sagri M, Tacconi P (1973) A geological map of Ethiopia and Somalia (1973) 1:2,000,000 and comment with a map of major landforms. National Council of Research, Roma

Meshesha D, Shinjo R, Matsumura R, Chekol T (2011) Metasomatised lithospheric mantle beneath Turkana depression in southern Ethiopia (the East Africa Rift): geochemical and Sr–Nd–Pb isotopic characteristics. Contrib Mineral Petrol 162:889–907

Morimoto N (1988) Nomenclature of pyroxenes. Am Mineral 73:1123–1133

Nasir S (1992) The lithosphere beneath the northwestern part of the Arabian Plate Jordan. Evidence from xenoliths and geophysics. Tectonophysics 201:357–370

Nasir S, Rollinson H (2009) The nature of the subcontinental lithospheric mantle beneath the Arabian shield: mantle xenoliths from southern Syria. Gondwana Res 172(3–4):323–333

Nasir S, Stern R (2012) Lithospheric petrology of the eastern Arabian plate: constraints from Al-Ashkhara (Oman) xenoliths. Lithos 32–33:98–112

Nasir S, Al-Sayigh A, Alharthy A, Al-Lazki A (2006) Geochemistry and petrology of Tertiary volcanic rocks and related ultramafic xenoliths from the central and Eastern Oman Mountains. Lithos 90:249–270

Nimis P, Taylor WR (2000) Single-clinopyroxene thermobarometry for garnet peridotites. Part I. Calibration and testing of a Cr-in-Cpx barometer and an enstatite-in-Cpx thermometer. Contrib Miner Petrol 139:541–554

Norman MD (1998) Melting and metasomatism in the continental lithosphere: laser ablation ICPMS analysis of minerals in spinel lherzolites from Eastern Australia. Contrib Mineral Petrol 130:240–255

Nowell GM, Kempton PD, Noble SR, Fitton JG, Saunders AD, Mahoney JJ, Taylor RN (1998) High precision Hf isotope measurements of MORB and OIB by thermal ionization mass spectrometry: insights into the depleted mantle. Chem Geol 149:211–233

O'Nions RK, Carter SR, Evensen NM, Hamilton PJ (1979) Geochemical and cosmochemical applications of Nd isotope analysis. Ann Rev Earth Planet Sci 7:11–38

Orlando A, Abebe T, Manetti P, Santo AP, Corti G (2006) Petrology of mantle xenoliths from Megado and Dillo, Kenya Rift, southern Ethiopia. Ofioliti 31:71–87

Ottonello G, Ernst WG, Joron JL (1984) Rare Earth element and 3rd transition element geochemistry of peridotitic rocks: i. peridotite from western Alps. J Petrol 25:343–372

Pearce NJG, Perkins WT, Westgate JA, Gorton MP, Jackson SE, Neal CR, Chenery SP (1997) A compilation of new and published major and trace element data for NIST SRM 610 and NIST SRM 612 glass reference materials. Geostand Geoanal Res 21(1):115–144

Pearson DG (1999) The age of continental roots. Lithos 48:171–194

Piccardo GB, Müntener O, Zanetti A, Pettke T (2004) Ophiolitic peridotites of the Alpine-Apennine system: mantle processes and geodynamic relevance. Int Geol Rev 46:1119–1159

Piccardo GB, Zanetti A, Müntener O (2007) Melt/peridotite interaction in the southern Lanzo peridotite: field, textural and geochemical evidence. Lithos 94:181–209

Pollack H, Chapman D (1977) On the regional variation of heat flow, geotherms, and lithospheric thickness. Tectonophysics 38(3–4):279–296

Powell W, O'Reilly S (2007) Metasomatism and sulfide mobility in lithospheric mantle beneath eastern Australia: implications for mantle Re–Os chronology. Lithos 94:132–147

Raczek I, Jochum KP, Hofmann AW (2003) Neodymium and Strontium isotope data for USGS reference materials BCR-1, BCR-2, BHVO-1, BHVO-2, AGV-1, AGV-2, GSP-1, GSP-2 and eight MPI-DING reference glasses. Geostand Newsl 27:173–179

Rampone E, Romairone A, Hofmann AW (2004) Contrasting bulk and mineral chemistry in depleted peridotites: evidence for reactive porous flow. Earth Planet Sci Lett 218:491–506

Reisberg L, Lorand JB, Bedini RM (2004) Reliability of Os model ages in pervasively metasomatized continental lithosphere: a case study of Sidamo spinel peridotite xenoliths (East African Rift, Ethiopia). Chem Geol 208:119–140

Rogers S, Dautria JM, Coulon C, Pik R, Yirgu G, Michard A, Legros P, Ayalew D (1999) An insight on the nature, composition and evolution of the lithospheric mantle beneath the North-western Ethiopian plateau; the ultrabasic xenoliths from the Tana Lake Province. Acta Vulcanol 11:161–168

Rooney O, Furman T, Yirgu G, Ayalew D (2005) Structure of Ethiopian lithosphere: xenoliths evidence in the Main Ethiopian Rift. Geochim Cosmochim Acta 69:3889–3910

Rudnick RL, McDonough WL, Chappell BW (1993) Carbonatite metasomatism in the northern Tanzanian mantle: petrographic and geochemical characteristics. Earth Planet Sci Lett 114:463–475

Rudnick RL, Gao S, Ling WL, Liu YS, McDonough WF (2004) Petrology and geochemistry of spinel peridotite xenoliths from Hannuoba and Qixia, North China Craton. Lithos 77:609–637

Sachtleben TH, Seck HA (1981) Chemical control of Al-solubility in orthopyroxene and its implications on pyroxene geothermometry. Contrib Mineral Petrol 78:157–165

Shaw CJ (1997) Origin of sulfide blebs in variably metasomatized mantle xenoliths, Quaternary West Eifel Volcanic field, Germany. Can Mineral 35:1453–1463

Shaw JE, Baker JA, Kent AJR, Ibrahim KM, Menzies MA (2007) The geochemistry of the Arabian lithospheric mantle—source for intraplate volcanism? J Petrol 48:1495–1512

Shinjo R, Chekol T, Meshesha D, Tatsumi Y, Itaya T (2010) Geochemistry and geochronology of the mafic lavas from the southeastern Ethiopian rift (the East African Rift system): assessment of models on magma sources, plume-lithosphere interaction and plume evolution. Contrib Mineral Petrol 162:209–230

Stern M, Abdelsalam M (1998) Formation of juvenile continental crust in the Arabian-Nubian shield: evidence from granitic rocks of the Nakasib suture, NE Sudan. Geol Rundsch 87:150–160

Stern M, Goldstein S (1996) From plume head to continental lithosphere in the Arabian–Nubian shield. Nature 382:773–778

Stern RJ, Johnson P (2010) Continental lithosphere of the Arabian plate: a geologic, petrologic, and geophysical synthesis. Earth Sci Rev 101:29–67

Stern R, Kröner A (1993) Late Precambrian crustal evolution in NE Sudan: isotopic and geochronologic constraints. J Geol 101:555–574

Streckeisen A (1976) To each plutonic rock its proper name. Earth Sci Rev 12:1–33

Su BX, Zhang HF, Sakyi PA, Yang YH, Ying JF, Tang YJ, Qin KZ, Xiao Y, Zhao XM, Mao Q, Ma YG (2011) The origin of spongy texture of mantle xenolith minerals from the Western Qinling, Central China. Contrib Mineral Petrol 161:465–482

Sun SS, McDonough WF (1989) Chemical and isotopic systematic of oceanic basalts: implications for mantle compositions and processes. Geol Soc Spec Publ 42:313–345

Tanaka R, Nakamura E (2002) Geochemical evolution of Koolau Volcano, Hawaii. In: Takahashi E, Lipman PW, Garcia MO, Naka J, Aramaki S (eds) Hawaiian volcanoes: deep underwater perspective, geophysics monogr, vol 128., AGU geophys monographWashington, DC, pp 311–332

Tang YJ, Zhang HF, Ying JF, Zhang J, Liu XM (2008) Re-fertilization of ancient lithospheric mantle beneath the central North China Craton: evidence from petrology and geochemistry of peridotite xenoliths. Lithos 101(3–4):435–452

Teklay M, Scherer EE, Mezger K, Danyushevsky L (2010) Geochemical characteristics and Sr–Nd–Hf isotope compositions of mantle xenoliths and host basalts from Assab, Eritrea: implications for the composition and thermal structure of the lithosphere beneath the Afar depression. Contrib Mineral Petrol 159:731–751

Tommasini S, Manetti P, Innocenti I, Sintoni MF, Conticelli S, Abebe T (2005) The Ethiopian subcontinental mantle domains: geochemical evidence from Cenozoic massif lavas. Mineral Petrol 84:259–281

Vervoort JD, Blichert-Toft J (1999) Evolution of the depleted mantle: Hf isotope evidence from juvenile rocks through time. Geochim Cosmochim Acta 63:533–556

Vervoort J, Patchett P, Blichert-Toft J, Albarede F (1999) Relationships between Lu–Hf and Sm–Nd isotopic systems in the global sedimentary system. Earth Planet Sci Lett 168:79–99

Wasserburg G, Jacousen S, DePaolo D, McCulloch M, Wen T (1981) Precise determination of ratios, Sm and Nd isotopic abundances in standard solutions. Geochim Cosmochim Acta 45:2311–2323

Wells PRA (1977) Pyroxene thermometry in simple and complex systems. Contrib Mineral Petrol 62:129–139

Windley B, Whitehouse M, Ba-Bttat M (1996) Early precambrian gneiss terranes and Pan-African island arc in Yemen: crustal accretion of the Eastern Arabian shield. Lithos 24:131–134

Witt-Eickschen E, Seck HA (1991) Solubility of Ca and Al in orthopyroxene from spinel peridotite: an improved version of an empirical geothermometer. Contrib Mineral Petrol 106:431–439

Yang YH, Zhang HF, Chu ZY, Lie-wen X, Wu FY (2010) Combined chemical separation of Lu, Hf, Rb, Sr, Sm and Nd from a single rock digest and precise and accurate isotope determinations of Lu–Hf, Rb–Sr and Sm–Nd isotope systems using multi-collector ICP-MS and TIMS. Int J Mass Spectrom 290:120–126

Yaxley GM, Crawford AJ, Green DH (1991) Evidence for carbonatite metasomatism in spinel peridotite xenoliths from Western Victoria, Australia. Earth Planet Sci Lett 107(2):305–317

Yemane T, WoldeGebriel G, Tesfaye S, Berhe SM, Durary S, Ebinger CJ, Kelley S (1999) Temporal and geochemical characteristics of Tertiary volcanic rocks and tectonic history in the southern Main Ethiopian Rift and adjacent volcanic fields. Acta Vulcanol 11:99–119

Zhang HF, Goldstein SL, Zhou XH, Sun M, Zheng JP, Cai Y (2008) Evolution of subcontinental lithospheric mantle beneath Eastern China: Re–Os isotopic evidence from mantle xenoliths in Paleozoic kimberlites and Mesozoic basalts. Contrib Mineral Petrol 155:271–293

Zhang HF, Deloule E, Tang YJ, Ying JF (2010) Melt/rock interaction in remains of re-fertilized Archean lithospheric mantle in Jiaodong Peninsula, North China Craton: Li isotopic evidence. Contrib Mineral Petrol 160:261–277

Zhang HF, Sun YL, Tang YJ, Xiao Y, Zhang H, Zhao XM, Santosh M, Menzies MA (2012) Melt-peridotite interaction in the Precambrian mantle beneath the Western North China Craton: petrology, geochemistry and Sr, Nd and Re isotopes. Lithos 149:100–114

Zheng JP, O'Reilly SY, Griffin WL, Lu FX, Zhang M, Pearson NJ (2001) Relics of refractory mantle beneath the eastern North China block: significance for lithosphere evolution. Lithos 57:43–66

Zheng JP, Griffin WL, O'Reilly SY, Yu CM, Zhang HF, Pearson N, Zhang M (2007) Mechanism and timing of lithospheric modification and replacement beneath the eastern North China Craton: Peridotitic xenoliths from the 100 Ma Fuxin basalts and a regional synthesis. Geochim Cosmochim Acta 71:5203–5225